Primate TRIM5 proteins form hexagonal nets on HIV-1 capsids

Yen-Li Li[1†], Viswanathan Chandrasekaran[1†], Stephen D. Carter[2], Cora L. Woodward[2], Devin E Christensen[1], Kelly A. Dryden[3], Owen Pornillos[3], Mark Yeager[3], Barbie K. Ganser-Pornillos[3*], Grant J. Jensen[2,4*], Wesley I. Sundquist[1*]

[1]Department of Biochemistry, University of Utah, Salt Lake City, UT 84112, USA; [2]Division of Biology and [4]Howard Hughes Medical Institute, California Institute of Technology, Pasadena, CA 91125, USA; [3]Department of Molecular Physiology and Biological Physics, University of Virginia School of Medicine, Charlottesville, VA 22908, USA

[†]These authors contributed equally, *Co-corresponding authors

ABSTRACT

TRIM5 proteins are restriction factors that block retroviral infections by binding viral capsids and preventing reverse transcription. Capsid recognition is mediated by C-terminal domains on TRIM5α (SPRY) or TRIMCyp (cyclophilin A), which interact weakly with capsids. Efficient capsid recognition also requires the conserved N-terminal tripartite motifs (TRIM), which mediate oligomerization and create avidity effects. To characterize how TRIM5 proteins recognize viral capsids, we developed methods for isolating native recombinant TRIM5 proteins and purifying stable HIV-1 capsids. Biochemical and EM analyses revealed that TRIM5 proteins assembled into hexagonal nets, both alone and on capsid surfaces. These nets comprised open hexameric rings, with the SPRY domains centered on the edges and the B-box and RING domains at the vertices. Thus, the principles of hexagonal TRIM5 assembly and capsid pattern recognition are conserved across primates, allowing TRIM5 assemblies to maintain the conformational plasticity necessary to recognize divergent and pleomorphic retroviral capsids.

INTRODUCTION

Mammalian hosts have evolved a series of different innate immune strategies to combat retroviruses (reviewed in (Altfeld and Gale, 2015; Bieniasz, 2003, 2004; Fitzgerald et al., 2014; Harris et al., 2012; Neil and Bieniasz, 2009; Rustagi and Gale, 2014; Sparrer and Gack, 2015; van Montfoort et al., 2014; Yoo et al., 2014)). TRIM5α and the related TRIMCyp protein (collectively TRIM5) are restriction factors that recognize the capsid surfaces of incoming retroviral core particles, induce their dissociation, and inhibit reverse transcription (Sayah et al., 2004; Stremlau et al., 2004; Stremlau et al., 2006). The mechanistic basis for core inactivation is not yet well established, but current models invoke the involvement of proteasomes (Anderson et al., 2006; Campbell et al., 2008; Diaz-Griffero et al., 2007; Kutluay et al., 2013; Lukic et al., 2011; Rold and Aiken, 2008; Wu et al., 2006), autophagosomes (Mandell et al., 2014a; Mandell et al., 2014b), and/or the establishment of a general antiviral state (Pertel et al., 2011).

Like other members of the tripartite motif (TRIM) family (Reymond et al., 2001), TRIM5 proteins comprise a RING E3 ubiquitin (Ub) ligase domain (Meroni and Diez-Roux, 2005; Yamauchi et al., 2008), an L1 linker, a B-box 2 self-assembly domain (Diaz-Griffero et al., 2009; Javanbakht et al., 2005; Li and Sodroski, 2008), an antiparallel dimeric coiled-coil, and an L2 linker that folds back on the coiled-coil (Goldstone et al., 2014; Li et al., 2014; Sanchez et al., 2014; Weinert et al., 2015) (Figure 1A). TRIM5 proteins also contain one of two different C-terminal viral core recognition domains, a B30.2/SPRY domain in TRIM5α (hereafter termed SPRY) or a cyclophilin A (CypA) domain in TRIMCyp (Brennan et al., 2008; Newman et al., 2008;

Nisole et al., 2004; Sayah et al., 2004; Stremlau et al., 2006; Stremlau et al., 2005; Virgen et al., 2008).

TRIM5 proteins act by binding the outer capsid shell of the viral core (Biris et al., 2013; Black and Aiken, 2010; Diaz-Griffero et al., 2006b; Kar et al., 2008; Kovalskyy and Ivanov, 2014; Langelier et al., 2008; Sayah et al., 2004; Sebastian and Luban, 2005; Stremlau et al., 2006; Zhao et al., 2011). The capsid protects and organizes the internal ribonucleocapsid, which comprises the viral NC protein, the RNA genome, and associated replicative enzymes. Closed retroviral capsids are constructed from several hundred CA protein hexamers and exactly 12 CA pentamers ((Ganser et al., 1999; Gres et al., 2015; Li et al., 2000; Obal et al., 2015; Pornillos et al., 2011; Zhao et al., 2013) and reviewed in (Ganser-Pornillos et al., 2012; Zhang et al., 2015)). Although all retroviral capsids are organized following these principles, individual capsids are unique, asymmetric objects that can differ in hexamer numbers and pentamer distributions (Benjamin et al., 2005; Briggs et al., 2006; Butan et al., 2008; Ganser-Pornillos et al., 2004; Heymann et al., 2008). For example, HIV-1 capsids are typically conical, but their sizes and cone angles can vary, and cylindrical and spherical capsids also form (Benjamin et al., 2005; Briggs et al., 2006; Briggs et al., 2003; Ganser-Pornillos et al., 2004; Heymann et al., 2008; Welker et al., 2000). Indeed, spherical and cylindrical capsids predominate in other retroviral genera, and capsid surface properties can vary considerably because CA proteins from different genera share low sequence identity (Berthet-Colominas et al., 1999; Campos-Olivas et al., 2000; Cornilescu et al., 2001; Ganser et al., 1999; Jin et al., 1999; Khorasanizadeh et al., 1999; Kingston et al.,

2000; Momany et al., 1996; Mortuza et al., 2008; Mortuza et al., 2004; von Schwedler et al., 1998; Zlotnick et al., 1998).

To function effectively, individual TRIM5 proteins must overcome these variations in retroviral capsid shape and sequence (Hatziioannou et al., 2003; Wilson et al., 2008). We, and others, have proposed that TRIM5 proteins recognize pleomorphic capsids by recognizing repeating patterns on the capsid surface (Biris et al., 2012; Ganser-Pornillos et al., 2011; Goldstone et al., 2014; Yang et al., 2012). This model supposes that flexible loops on the SPRY and CypA domains can adopt multiple different conformations and can bind weakly to conserved elements on the capsid surfaces (Biris et al., 2012; Caines et al., 2012; Kovalskyy and Ivanov, 2014; Price et al., 2009; Song et al., 2005a; Stremlau et al., 2005; Ylinen et al., 2010). These weak interactions are then amplified by TRIM5 assembly into a higher-order hexagonal lattice, which positions arrays of SPRY/CypA domains to interact with repeating epitopes on the capsid surfaces (Ganser-Pornillos et al., 2011; Li and Sodroski, 2008).

This “pattern recognition” model has been supported by biochemical and structural analyses of a TRIM5 protein construct called TRIM5-21R, which is an artificial chimera in which the RING domain from human TRIM21 replaces the RING domain of rhesus TRIM5α (Diaz-Griffero et al., 2006a; Kar et al., 2008; Langelier et al., 2008). The TRIM5-21R construct retains HIV-1 restriction activity, and has been used in several studies owing to its unusually favorable stability, solubility and assembly properties. Consistent with the pattern recognition model, TRIM5-21R was shown to assemble into open hexagonal lattices, both alone and on the surface of 2D CA crystals that mimic the surface of the HIV-1 capsid (Ganser-Pornillos et al., 2011). TRIM5-21R assemblies

could be microns in size but lacked strict long-range order, and 2D projections could therefore only be reconstructed to a resolution of ~7.5 nm. Domain positions therefore had to be inferred, and were interpreted in the absence of high-resolution information on the structure of the TRIM5 protein core.

Technical challenges in purifying authentic HIV-1 cores have also been a significant experimental limitation, and all published biochemical and structural studies of TRIM5α-capsid interactions have therefore either employed crude viral core preparations or artificial mimics of the capsid surface (Black and Aiken, 2010; Ganser-Pornillos et al., 2011; Langelier et al., 2008; Sebastian and Luban, 2005; Stremlau et al., 2006; Zhao et al., 2011). Thus, the interactions between authentic viral capsids and TRIM5 proteins have yet to be investigated biochemically or structurally. To address these different shortcomings, we have developed methods for preparing authentic recombinant TRIM5 proteins, co-assemblies of TRIM5 and CA proteins, and stable HIV-1 cores. These reagents were then used to demonstrate that TRIM5 proteins form hexagonal arrays on HIV-1 capsids.

RESULTS

Structure-based models for TRIM5-21R assembly

A composite model for the domain organization within TRIM5α is shown in Figure 1A. We (Sanchez et al., 2014), and others (Goldstone et al., 2014; Weinert et al., 2015), have suggested that these dimers form the edges of the hexameric rings observed within the hexagonal TRIM5-21R lattice (modeled in Figure 1B). This model is attractive because the edges of each hexagon are ~19 nm long, which would accommodate the antiparallel TRIM5α coiled-coil (~17 nm), and the RING domain would associate at the three-fold vertices, which is consistent with the trimeric B-box 2 domain structure presented in the accompanying paper (Wagner et al., 2016). Finally, the L2 linkers fold back and form a four-helix bundle at the center of the coiled-coil and this platform could, in principle, buttress and orient the TRIM5α SPRY domains. None of the domain positions have been determined experimentally, however and we therefore began our studies by defining the location of the SPRY domains within the hexagonal TRIM5-21R lattice.

To visualize TRIM5-21R assemblies in three dimensions and define the SPRY domain positions, we generated electron cryotomograms (ECT) from tilt series of vitrified 2D crystals of both full length TRIM5-21R (Figure 1C) and a construct that lacked the SPRY domain (TRIM5-21R$_{\Delta SPRY}$, residues 1-300, Figure 1D). The 3D reconstructions were refined and improved by subtomogram averaging of densities centered at equivalent lattice vertices. As expected, TRIM5-21R and TRIM5-21R$_{\Delta SPRY}$ both assembled into similar planar lattices of hexagonal rings, with inter-ring spacings and protein densities matching those of the previous 2D projection structures (Ganser-

Pornillos et al., 2011). Difference density maps clearly revealed that the SPRY domains are located at the center of each hexagon edge (Figure 1E), thereby supporting the model shown in Figure 1B.

The TRIM5-21R lattice is a hexagonal net with variable arm lengths and angles

Although the paracrystalline arrays of TRIM5-21R exhibited long-range order, they diffracted poorly, suggesting variability within the lattice. To quantify this variability, we performed a nearest neighbor analysis of the refined positions of the lattice vertices used for subtomogram averaging. The relative positions of 153 vertices in the TRIM5-21R 2D crystals were used to define individual hexamer edge lengths and angles (see Figure 1F). The length distribution of hexamer edges was centered about a mean of 19 nm, but individual lengths varied by up to ±5 nm (Figure 1G, upper panel). Similarly, the distribution of hexamer vertex angles was centered about 120°, but varied by up to ±20°. Thus, individual rings within the TRIM5 lattice exhibited considerable conformational variability, explaining the poor crystalline order and modest diffraction resolution.

Expression and purification of authentic primate TRIM5α and TRIMCyp proteins

Recombinant owl monkey TRIMCyp has been purified (Pertel et al., 2011), but TRIM5α proteins are more challenging to purify because these proteins tend to self-assemble, both in cells and *in vitro*. Hence, previous biochemical and structural studies of TRIM5α proteins have been performed with impure proteins, protein fragments, or non-native chimeric constructs (Biris et al., 2012; Goldstone et al., 2014; Kar et al.,

2008; Langelier et al., 2008; Sanchez et al., 2014; Yang et al., 2012; Yudina et al., 2015). To overcome this limitation, we tested a variety of different expression and purification conditions, with the goal of developing a general method for preparing milligram quantities of authentic, full-length primate TRIM5α and TRIMCyp proteins.

The strategy that was ultimately successful entailed expressing TRIM5 proteins in insect cells using a baculoviral expression system. As described in greater detail in the Experimental Methods, expressed TRIM5 proteins formed cytoplasmic bodies that could be solubilized by lysing the cells in a low ionic strength, alkali buffer that contained the non-ionic detergent Triton X-100, as well as a non-detergent small molecule, sulfobetaine-256 (NDSB-256) that has previously been shown to inhibit protein aggregation (Sainsbury et al., 2008; Vuillard et al., 1995). Once solubilized, primate TRIM5 proteins typically remained dimeric and soluble under low salt, alkaline conditions in the absence of Triton X-100 and NDSB-256, even at concentrations greater than 1 mg/ml. The proteins could therefore be purified, provided they were maintained at high pH, low salt and/or low protein concentrations.

Our stepwise protein purification protocol is illustrated for rhesus TRIM5α in Figure 2A. Briefly, various N-terminal OneSTrEP-FLAG- (OSF-) or C-terminal FLAG-OneSTrEP- (FOS-) tagged TRIM5 proteins were initially purified using Strep-Tactin affinity chromatography, the affinity tag was removed by PreScission protease treatment, and the proteins were then purified to homogeneity by anion exchange and gel filtration chromatography. Analogous approaches were used to express and purify wild type and mutant TRIM5α proteins from rhesus macaques (*Macaca mulatta*, here abbreviated TRIM5α_{rh}), African green monkeys (*Chlorocebus pygerythrus*,

183 TRIM5α$_{AGMpyg}$), chimpanzees (*Pan troglodytes*, TRIM5α$_{cpz}$), humans (*Homo sapiens*,
184 TRIM5α$_{hu}$), and the TRIMCyp protein from owl monkeys (*Aotus trivirgatus*, TRIMCyp).
185 Yields ranged between 1.3 and 9.6 mg/L of insect cell cultures, and all of the proteins
186 eluted with similar retention times during the final gel filtration chromatography step,
187 indicating that they were all dimers of similar shape. All of the proteins could be purified
188 to >95% purity (Figure 2B) with the exception of TRIMCyp, where our preparations also
189 contained breakdown contaminants that mapped to proteolytic cleavage at residues
190 Lys283 and Gln287 (not shown). These breakdown contaminants were eliminated by
191 creating a mutant construct that expressed TRIMCyp$_{K283D,Q287D}$ (Figure 2B, lane 4).
192 These mutations are not expected to affect functionally relevant properties of the protein
193 because TRIMCyp$_{K283D,Q287D}$ retains potent HIV-1 restriction activity (Figure 2 – figure
194 supplement 1).
195
196 **Conservation of hexagonal TRIM5 protein assembly**
197 To determine whether the ability to assemble into hexagonal nets is a conserved
198 property of authentic TRIM5 proteins, we screened for conditions that promoted
199 assembly of different primate TRIM5 proteins, using negative stain EM imaging to assay
200 assembly states. These screens identified conditions under which two of the TRIM5
201 proteins, TRIM5α$_{AGMpyg}$ (Figure 2C) and TRIMCyp (Figure 2D) spontaneously formed
202 2D hexagonal assemblies that were similar in appearance to those formed by TRIM5-
203 21R (Ganser-Pornillos et al., 2011). Assembly efficiencies varied, however, as
204 TRIM5α$_{AGMpyg}$ assembled very efficiently under the same conditions as TRIM5-21R,
205 whereas TRIMCyp assembled inefficiently and required additional precipitants (see

Materials and methods). Negatively stained 2D crystals of TRIM5α$_{AGMpyg}$ and TRIMCyp were imaged and processed to generate Fourier-filtered 2D projection reconstructions (Figure 2C, D; bottom). Both TRIM5 proteins formed lattices comprising open hexameric rings that were similar in appearance and size to the TRIM5-21R rings, demonstrating that diverse TRIM5 proteins from different primates that share 73% pairwise identity across their TRIM domains share the ability to assemble into analogous hexagonal nets.

Templated hexagonal TRIM5 protein assembly on HIV-1 CA surfaces

The pattern recognition model for TRIM5 restriction predicts that binding to the surface of the viral capsid promotes hexagonal TRIM5 assembly. We therefore tested whether hexagonal 2D crystals of HIV-1 CA, which mimic the capsid surface, could promote the assembly of three different restricting TRIM5 proteins; TRIM5α$_{rh}$, TRIMCyp$_{K283D,Q287D}$, and TRIM5α$_{hu,R332P}$, and two different non-restricting TRIM5 proteins; wild type TRIM5α$_{hu}$ and TRIM5α$_{cpz}$ (Hatziioannou et al., 2004; Nisole et al., 2004; Sayah et al., 2004; Song et al., 2005b; Stremlau et al., 2004; Stremlau et al., 2005; Yap et al., 2005). To test for templated assembly of TRIM5 proteins, soluble dimeric proteins were incubated together with preassembled 2D CA crystals under solution conditions that were sufficiently stringent to prevent untemplated assembly. TRIM5α$_{AGMpyg}$ was not used in these studies because it assembled very robustly even in the absence of a template.

As shown in Figure 3, the three restricting TRIM5 proteins assembled into visible hexagonal nets on the surfaces of preformed HIV-1 CA crystals, whereas templated

assembly was not observed for either one of the non-restricting TRIM5 proteins (Figure 3C and data not shown). Templated assembly therefore correlated well with restriction activity, emphasizing the coupling of CA binding and TRIM5 lattice assembly. Computed Fourier transforms of the images of decorated crystals (Figure 3, insets) revealed well-defined first- and second-order reflections from the smaller underlying CA lattice (red and blue), as well as more diffuse peaks (TRIM5α_{rh} and TRIMCyp$_{K283D,Q287D}$, green) or a powder diffraction ring (TRIM5$\alpha_{hu,R332P}$) corresponding to the first-order reflections from the hexagonal TRIM5 lattices. Thus, all three restricting TRIM5 proteins bound the CA surfaces and assembled into hexagonal nets that were clearly visible, but lacked extensive crystalline order.

TRIM5 binding to helical HIV-1 CA tubes

The helical tubes formed by pure recombinant HIV-1 CA provide another regularized model for the curved, symmetric arrays of CA hexagons on conical viral capsid surfaces (Campbell and Vogt, 1995; Li et al., 2000). We employed a sucrose co-sedimentation assay to test whether the restricting TRIM5α_{AGMpyg} and TRIMCyp$_{K283D,Q287D}$ proteins bound disulfide-crosslinked helical tubes formed by a mutant HIV-1 CA protein that assembled into discrete helical tubes stabilized by intrahexamer disulfide crosslinks (CA$_{A14C,E45C,A92E}$) (Byeon et al., 2009; Ganser-Pornillos et al., 2011; Langelier et al., 2008; Li et al., 2000; Pornillos et al., 2010; Pornillos et al., 2009; Zhao et al., 2011). Both TRIM5α_{AGMpyg} and TRIMCyp$_{K283D,Q287D}$ bound the CA tubes, as judged by their co-sedimentation through the sucrose cushion when the CA tubes were present, but not when they were absent (compare the “pellet” fractions in

lanes 1 vs. 2 and lanes 5 vs. 6 in Figure 4 – figure supplement 1A). Binding was specific because TRIM5α$_{AGMpyg}$ did not co-sediment with CA tubes when the SPRY domain was removed (compare lanes 2 vs. 4) and because TRIMCyp$_{K283D,Q287D}$ did not co-sediment with CA tubes in the presence of cyclosporine A, which competitively inhibits the CypA-CA interaction (compare lanes 6 vs. 7). Thus, pure recombinant TRIM5 proteins bind the hexagonal lattices of both helical CA tubes and 2D CA crystals.

Negative stain and deep-etch electron microscopy were used to image the TRIM5-decorated HIV-1 CA tubes. Four restricting TRIM5 proteins, TRIM5α$_{AGMpyg}$, TRIM5α$_{rh}$, TRIMCyp$_{K283D,Q287D}$, and TRIM5α$_{hu,R332P,}$ formed thin ring-like decorations on the surfaces of CA tubes (Figure 4 – figure supplement 1B). The TRIM5 decorations typically appeared as light, string-like nets against the darker underlying CA tubes when the assemblies were stained with either uranyl acetate (UA) or phosphotungstate (PTA). Equivalent decorations were not observed for control CA tubes alone or for CA tubes plus TRIM5α$_{hu,}$ which does not restrict HIV-1. TRIM5 decoration of CA tubes therefore correlated with restriction activity.

Deep-etch EM images often exhibit even greater contrast than negative stain transmission EM images, and this effect was evident in deep-etch images of undecorated HIV-1 CA tubes, where rows of individual CA hexamers were readily visible (Figure 4A, upper panel). Strings and rings of TRIM5α$_{AGMpyg}$ were often readily visible on the decorated CA tube surfaces, and networks of rings were sometimes observable (Figure 4A, lower panel). Hence, TRIM5 proteins can form hexagonal nets on the surfaces of helical HIV-1 CA tubes.

The efficiency of TRIM5 assembly on disulfide-crosslinked CA tubes was relatively low, which may explain why the decorations were not noted in previous studies. We therefore screened additional assembly conditions to determine the source of this variability. These experiments revealed that co-incubation of native CA protein with TRIM5α under low ionic strength conditions produced CA tubes that were extensively decorated with TRIM5α. Co-assembly was reproducible, and both tagged and untagged TRIM5-21R, $TRIM5_{AGMpyg}$, and $TRIM5_{rh}$ proteins formed ring-like decorations on CA tube surfaces at a variety of different CA/TRIM5 molar ratios (Figure 4B, data not shown, and Wagner et al., 2016). $TRIM5\alpha_{AGMpyg}$ inter-ring spacing distribution on the tubes centered at 30-35 nm, as was also the case for $TRIM5\alpha_{AGMpyg}$ assemblies on pre-formed disulfide-crosslinked CA tubes (Figure 4C). In all cases, the rings were irregular and their spacings varied between 15 and 55 nm. Electron cryotomography (ECT) analyses similarly revealed extensive networks of hexagonal nets coating individual cylinders (Figure 4D and Video 1). As seen previously for TRIM5-21R 2D crystals (Ganser-Pornillos et al., 2011), the hexamer edge lengths measured from three-fold vertices selected from the tomogram were predominantly ~19 nm, but varied between 15 to 23 nm. Similarly, the hexamer vertex angles averaged ~120°, but ranged from 80° to 160° (Figure 4E). The flexibility of the TRIM5 assembly may reflect flexing of the coiled-coil domains and/or the hinge between B-box 2 and coiled-coil domains (Wagner et al., 2016). In summary, TRIM5 proteins consistently formed hexagonal arrays on curved HIV-1 CA lattices, and the TRIM5 lattice was more extensive when the two proteins co-assembled together, presumably because the two lattices could template one another and thereby optimize their interactions.

297

298 **Generation of hyperstable, disulfide-crosslinked HIV-1 core particles**

299 A central goal of our studies was to analyze TRIM5 binding to authentic viral
300 capsids, both biochemically and by direct imaging. This goal is technically challenging
301 owing to the inherent instability of viral core particles. We reasoned that this challenge
302 might be overcome by disulfide-crosslinking the capsid shell to increase its stability.
303 This strategy was particularly attractive because previous studies showed that Cys
304 residues substituted at CA positions Ala14 and Glu45 crosslinked efficiently when CA
305 hexamers were assembled *in vitro* (Pornillos et al., 2010; Pornillos et al., 2009). We
306 therefore tested the effect of introducing these substitutions into authentic HIV-1
307 capsids.

308 Normal levels of viral particles were produced from 293T cells that expressed an
309 HIV-1_{NL4-3}ΔR8.2 proviral expression vector that encoded the mutant $CA_{A14C,E45C}$ protein
310 (not shown). Wild type and mutant viral cores were isolated by centrifuging virions
311 through a detergent layer to remove the outer viral membrane and then directly into a
312 30-70% sucrose gradient, where viral cores concentrated at a density of 1.22-1.27 g/ml
313 (fractions 10-12, highlighted in pink in Figure 5A) . As reported previously (Forshey et
314 al., 2002; Kotov et al., 1999), wild type cores could also be isolated using this procedure
315 (see Figure 5B). However, recovered core yields were consistently modest in our hands
316 (0.2±0.1% based upon total virion CA), apparently because most of the CA molecules
317 dissociated from the core and migrated to the top of the gradient during purification
318 (Figure 5A, left panel). In contrast, nearly all of the $CA_{A14C,E45C}$ protein migrated toward
319 the bottom of the gradient when cores were isolated from mutant virions (Figure 5A,

right panel). Much of this CA protein was present within small incomplete, broken, or spherical assemblies that concentrated at densities of 1.18-1.21 g/ml (gradient fractions 6-9, Figure 5A, right panel and see Figure 5 – figure supplement 1). These non-native assemblies probably arose from spurious crosslinking of CA hexamers in the free intraviral pool of CA molecules that are excluded from the mature HIV-1 capsid (Benjamin et al., 2005; Briggs et al., 2004; Lanman et al., 2004; Monroe et al., 2010). Nevertheless, a substantial fraction of the CA protein also concentrated at the density expected for native core particles (fractions 10-12, highlighted in pink in Figure 5A, right panel). These "hyperstable" cores were reproducibly recovered in higher yields (0.8±1%) than wild type cores (0.2±0.1%) and their morphologies were similar to wild type cores (Figure 5B, right panel). Consistent with the design, nearly all of the CA molecules within these fractions were crosslinked within stable hexamers, as analyzed by non-reducing SDS-PAGE and western blotting (Figure 5C). These experiments indicate that disulfide crosslinking occurs spontaneously in otherwise native and untreated HIV-1 capsids, and that the crosslinks stabilize the capsids without introducing any major morphological defects.

Isolation of HIV-1 core particles for cryoEM imaging

Hyperstable HIV-1 cores purified on sucrose gradients were not optimal for imaging studies because they aggregated and co-sedimented with vesicles and other impurities. To produce purer cores, we designed an alternative core affinity purification method that exploited the interaction between cyclophilin A (CypA) and HIV-1 CA (outlined in Figure 5 – figure supplement 1D) (Franke et al., 1994; Gamble et al., 1996;

343 Luban et al., 1993; Thali et al., 1994). Viral membranes were stripped by a brief Triton
344 X-100 treatment and the liberated cores were then captured on magnetic Strep-Tactin
345 beads derivatized with OSF-CypA. The immobilized cores were washed rigorously and
346 then eluted with the small molecule cyclosporine A (CsA), which competitively inhibits
347 the CypA-CA interaction and binds CypA ~700-fold more tightly than does CA (Figure
348 5D and Figure 5 – figure supplement 1E) (Braaten et al., 1996; Franke and Luban,
349 1996; Gamble et al., 1996; Wear et al., 2005; Yoo et al., 1997). This method increased
350 core yields by an additional 4-fold (3±2% core recovery) and increased their purity
351 (compare Figure 5D to Figure 5B, right panel). The method also reduced the fraction of
352 broken cores, possibly because they were less stable and therefore removed during the
353 extensive wash steps and/or because they bound less avidly to the matrix. To reduce
354 core clustering, we introduced the CA A92E substitution within the exposed loop of HIV-
355 1 CA. This mutation does not affect TRIM5α restriction (Li et al., 2006), and was
356 previously shown to reduce the clustering of helical CA tubes, presumably by reducing
357 overall surface hydrophobicity (Ganser-Pornillos et al., 2004; Li et al., 2000; Zhao et al.,
358 2011). As shown in Figure 5E, the substitution also reduced the clustering of viral cores
359 (compare Figures 5D and 5E), and did so without altering core morphology or reducing
360 core yields (3±1% core recovery).

361 In summary, dispersed hyperstable $CA_{A14C,E45C,A92E}$ cores could be purified by
362 affinity chromatography in high yields. The purified cores contained the expected viral
363 proteins as analyzed by SDS-PAGE with silver staining (Figure 5 – figure supplement
364 1F), were hyperstable and fully disulfide crosslinked (Figure 5C), exhibited normal
365 capsid morphologies (Figure 5B), and spread diffusely on EM grids (Figure 5E).

366

367 **TRIM5 binding to HIV-1 cores**

368 The susceptibility of different retroviruses to restriction by different TRIM5
369 variants can vary dramatically and appears to be determined largely at the level of
370 capsid recognition (Li et al., 2006; Ohkura et al., 2006; Perez-Caballero et al., 2005;
371 Sebastian and Luban, 2005; Song et al., 2005a; Stremlau et al., 2004; Stremlau et al.,
372 2006; Stremlau et al., 2005). Consistent with previous reports (Sayah et al., 2004; Song
373 et al., 2005b; Stremlau et al., 2004), we found that TRIM5 proteins restricted the
374 transduction of HeLa cells with an HIV-1 reporter vector, and the strength of restriction
375 followed the order: TRIMCyp and TRIMCyp$_{K283D,Q287D}$>TRIM5α$_{rh}$>TRIM5α$_{AGMpyg}$, with no
376 restriction observed for TRIM5α$_{cpz}$ or TRIM5α$_{hu}$ (Figure 2 – figure supplement 1). A
377 sucrose cushion co-sedimentation assay was again used to test whether pure
378 recombinant TRIM5α proteins bound directly to hyperstable HIV-1 cores, and whether
379 core binding correlated with restriction activity. These experiments were performed with
380 two proteins that restrict HIV-1, TRIM5α$_{AGMpyg}$ and TRIM5α$_{rh}$, and one that does not,
381 TRIM5α$_{cpz}$.

382 As shown in Figure 6A, the two restricting TRIM5α$_{AGMpyg}$ and TRIM5α$_{rh}$ proteins
383 both co-pelleted with hyperstable HIV-1 cores and did not pellet in the absence of cores
384 (compare lanes 1 vs. 2 and lanes 3 vs. 4). In contrast, the non-restricting TRIM5α$_{cpz}$
385 protein did not bind cores under the same conditions (compare lanes 5 vs. 6). These
386 core binding experiments were performed in the presence of excess TRIM5α proteins,
387 and the approximate stoichiometry of the pelleted core-TRIM5α$_{AGMpyg}$ complexes was
388 estimated by comparing the levels of CA and TRIM5α$_{AGMpyg}$ to standard curves of

known protein concentrations. The measured TRIM5α$_{AGMpyg}$:CA ratio in these experiments was 1:7±2 (n=4). Based upon their relative sizes, we estimate that each TRIM5 ring will cover ~14 CA hexamers (Ganser-Pornillos et al., 2011). Based upon an idealized binding model and the known stoichiometries of each ring (CA=6, TRIM5α=12) we estimate that a fully saturated capsid would have a TRIM5:CA ratio of ~1:14. Hence, two different restricting TRIM5α proteins can bind directly to hyperstable HIV-1 cores at near saturating levels *in vitro*, whereas the non-restricting TRIM5α$_{cpz}$ protein does not bind cores. Consistent with the solution binding experiments, negative stain electron microscopic images again revealed thin ring-like assemblies of TRIM5α$_{rh}$ proteins on the capsid surfaces of hyperstable viral cores (Figure 6B, compare the cores in the second and third rows with the undecorated cores in the first row).

EM imaging of TRIM5 decorated HIV-1 cores

Free and TRIM5α$_{AGMpyg}$-decorated cores were also visualized in three dimensions by ECT (Figure 7 and Figure 7 – figure supplement 1). Free hyperstable cores could be spherical, cylindrical, or conical, and general size distributions and lattice features were similar to native HIV-1 cores (Figure 7 – figure supplement 1). Holes in the tips of conical cores were also observed, supporting previous results suggesting that cores are frequently unclosed (Yu et al., 2013).

Samples in which cores were incubated with TRIM5α$_{AGMpyg}$ typically exhibited networks of densities at the air/water interface. These networks exhibited three-fold vertices in the plane of the interface that were similar to 2D hexagonal TRIM5α lattices but did not exhibit diffraction or crystalline order (Video 2). Approximately 12% of cores

imaged were also decorated on their outer capsid surfaces with TRIM5α$_{AGMpyg}$ densities. Multiple extended density "arms" approximately 19 nm in length were seen arranged in a roughly hexagonal pattern (Figure 7A, and Video 2).

The prevalence of TRIM5α$_{AGMpyg}$ at the air/water interface and relative paucity of TRIM5α-decorated cores suggested that previously core-bound TRIM5α was being lost to the air/water interface during plunge-freezing (Video 3). To reduce this problem, we crosslinked the core-TRIM5α complexes with ethylene glycol bis(sulfosuccinimidylsuccinate) (Sulfo-EGS) prior to plunge freezing. Even after crosslinking, a substantial amount of TRIM5α was still seen at the air/water interface, but now the majority of cores were decorated with TRIM5α$_{AGMpyg}$. Analysis of the volume surrounding these cores revealed broken, but extensive TRIM5α hexagonal nets, which in some cases enveloped the entire capsid (Figure 7B, Figure 7 – figure supplement 2, and Videos 4). TRIM5α nets on bona fide cores were again irregular, but exhibited similar distribution of hexamer edge lengths (20±2 nm, n=51) and vertex angles (120±2°, n=68) as CA/TRIM5 “co-assemblies” (Figure 7 – figure supplement 3). In some cases, TRIM5α densities with a length of ~ 38 nm were observed on the capsid surface (data not shown). These longer densities might occur through the association of two sets of TRIM5α dimers via dimeric rather than trimeric B-box 2 domain interactions (Wagner et al., 2016). Despite these irregularities, we were able to perform coarse, rigid body fitting of the crystal structures of B-box 2 trimers and coiled-coil dimers into 3D density maps. As shown in Figure 7C, each edge was occupied with a TRIM5α coiled-coil dimer and the three-fold densities were filled with three B-box 2 domains. The fitting revealed that TRIM5 hexagonal lattices are in good agreement with the crystal

structures in dimensions and angles. Overall, our results indicate that TRIM5 proteins form flexible hexagonal nets on the capsid surface with their domain positions schematically shown in Figure 7D.

DISCUSSION

Our studies further support the prevailing models that TRIM5 restriction factors bind directly to the surfaces of incoming retroviral capsids and that restriction susceptibility is dictated at the level of capsid recognition (Li et al., 2006; Ohkura et al., 2006; Perez-Caballero et al., 2005; Sebastian and Luban, 2005; Song et al., 2005a; Stremlau et al., 2004; Stremlau et al., 2006; Stremlau et al., 2005). In addition, we find that the ability to assemble into hexagonal nets comprising open, six-sided rings is a conserved feature of multiple different primate TRIM5 proteins. Our EM analyses, together with recent crystal structures of fragments of non-assembling TRIM proteins that span the core coiled-coil and L2 linker regions (Goldstone et al., 2014; Sanchez et al., 2014), indicate that each ring edge is formed by a TRIM5 dimer that displays two SPRY (or CypA) recognition domains at its center. Most importantly, we find that capsid binding and TRIM5 assembly are coupled processes that cooperate to promote the recognition of pleomorphic retroviral cores with high affinity and specificity.

Reagent development

Through the course of our studies we developed and characterized two new sets of reagents for studying retroviral replication and restriction: hyperstable, disulfide-crosslinked HIV-1 capsids and pure recombinant primate TRIM5 proteins. The generation of hyperstable capsids was enabled by previous studies showing that Cys residues at CA positions 14 and 45 form disulfide bonds efficiently *in vitro* when these residues are closely juxtaposed within the CA hexamer (Pornillos et al., 2010; Pornillos et al., 2009). Our experiments demonstrate that these disulfides also form efficiently in

464 the context of the intact HIV-1 capsid. A similar disulfide crosslinking strategy was also
465 used to link CA trimers at cysteine positions 207 and 216 across the local three-fold
466 axes of the HIV-1 capsid (Byeon et al., 2009; Zhao et al., 2011). We have compared
467 these two different systems, as well as an alternative strategy in which CA hexamers
468 were crosslinked by disulfide bonds between Cys residues at CA positions 42 and 54
469 (Pornillos et al., 2010). Disulfide bonds form readily within viral capsids in all three
470 cases (Byeon et al., 2009; Pornillos et al., 2010; Pornillos et al., 2009; Zhao et al., 2011)
471 (and data not shown), and we anticipate that the different crosslinking strategies could
472 have distinct advantages depending upon the application. For example, we have
473 confirmed the report that HIV-1 cores with trimerized CA proteins retain modest
474 infectivity (Byeon et al., 2009), whereas infectivity is almost completely abolished when
475 cores are crosslinked at either site in the CA hexamer. We also find, however, that viral
476 core yields and stabilities are greater for the two hexamer crosslinking systems, and are
477 highest for the Cys14/Cys45 system described here. Thus, these hyperstable capsids
478 should be optimal for analyzing the binding of a series of proteins and drugs that have
479 recently been described, including the proteins CPSF6 (Bhattacharya et al., 2014; Lee
480 et al., 2010; Price et al., 2014), Nup153 (Bhattacharya et al., 2014; Di Nunzio et al.,
481 2013; Matreyek et al., 2013; Price et al., 2014), and Nup358 (Bichel et al., 2013;
482 Meehan et al., 2014; Schaller et al., 2011), and the inhibitors PF-74 (Bhattacharya et al.,
483 2014; Blair et al., 2010; Fricke et al., 2013; Price et al., 2014) and BI-1 and BI-2 (Fricke
484 et al., 2014; Lamorte et al., 2013; Price et al., 2014). Hyperstable capsids may also
485 represent a useful starting point for the development of *in vitro* viral replication assays,

particularly if the capsid disulfides can be reduced without inactivating the internal reverse transcriptase and integrase enzymes.

The development of systems for producing milligram quantities of pure recombinant primate TRIM5 proteins should similarly facilitate studies of restriction by advancing methods for protein detection and enabling new mechanistic and structural analyses. For example, our recombinant TRIM5α_{rh} proteins have already been used successfully as antigens to generate monoclonal antibodies that can detect endogenous TRIM5α proteins (NIH AIDS Reagent Program, and (Imam et al., 2016)). Moreover, although structural studies of TRIM5 protein domains and fragments have made valuable contributions to our understanding of TRIM5 structure and enzymology, there are a number of indications that the different domains work together as an integrated machine (Ganser-Pornillos et al., 2011; Goldstone et al., 2014; Li et al., 2013; Li and Sodroski, 2008; Reymond et al., 2001; Sanchez et al., 2014). It will therefore also be important to study intact TRIM5 proteins, particularly to determine how capsid recognition is coupled to ubiquitin signaling (Fletcher et al., 2015; Pertel et al., 2011; Yudina et al., 2015).

TRIM5 recognition of retroviral capsids and its implications for restriction

Antiviral innate immune factors that function by recognizing retroviral capsids must overcome considerable sequence and structural variability. Primate TRIM5 proteins accomplish this task by coupling weak recognition of conserved capsid epitopes with hexagonal net assembly, thereby amplifying intrinsically weak binding affinities through avidity effects (Ganser-Pornillos et al., 2011; Price et al., 2009). Our

studies confirm that hexagonal net assembly is a conserved property, but also reveal that the TRIM5 hexagonal nets are not highly regular. The lack of strict regularity in the TRIM5 net may be required to adapt to the lack of regularity in the opposing retroviral capsids, where every CA hexagon occupies a slightly different local environment and where pentagons and other kinds of lattice “defects” are also prevalent (Byeon et al., 2009; Ganser-Pornillos et al., 2011; Gres et al., 2015; Hatziioannou et al., 2004; Obal et al., 2015; Pornillos et al., 2011; Yu et al., 2013; Zhao et al., 2013).

Consistent with a lattice assembly model, imaging studies have provided direct evidence that multiple TRIM5 molecules can bind continuously to incoming capsids, (Campbell et al., 2008; Danielson et al., 2012; Lukic et al., 2011). The stoichiometry of TRIM5-capsid interactions within cells is not yet known, but we find that TRIM5 molecules can cover most of the capsid surface *in vitro*. A patch of just 4-6 TRIM5 rings covers about half of the capsid surface (see Figure 7), however, and would present ~40 recognition domains for avid capsid binding. Thus, the entire capsid probably does not need to be completely enveloped within a surrounding TRIM5 lattice for restriction to occur. Indeed, CA mixing studies have shown that efficient TRIM5 restriction can occur even when only 25% of the capsid subunits are competent for TRIM5 binding (Shi et al., 2013).

TRIM5-mediated restriction appears to proceed via a multi-step pathway in which capsid recognition is followed by steps that lead to capsid dissociation and inhibition of reverse transcription (Pertel et al., 2011; Stremlau et al., 2006). In cells, the later processes can be decoupled from the initial binding event by treatment with proteasome inhibitors or by mutations in the RING domain (Anderson et al., 2006; Fletcher et al.,

2015; Kutluay et al., 2013; Roa et al., 2012; Wu et al., 2006). These treatments do not block TRIM5 binding, but presumably do interfere with ubiquitin-mediated signaling events. Thus, although TRIM5 binding can destabilize helical CA tubes *in vitro* (Black and Aiken, 2010; Zhao et al., 2011), capsid dissociation and inhibition of reverse transcription appear to require ubiquitin-dependent signaling in cells (Campbell et al., 2015; Fletcher et al., 2015). Capsid binding can activate TRIM5 ubiquitin E3 ligase activity *in vitro* (Pertel et al., 2011), and the structure of the hexagonal TRIM5 lattice suggests how this could occur. Recent structural studies of the RING domains from TRIM37 (PDB ID: 3LRQ) and TRIM5α (PDB ID: 4TKP) (Yudina et al., 2015) have demonstrated that the RING domains function as dimers. However, the antiparallel structure of the TRIM5 coiled-coil precludes close contact of the two RING domains within a single TRIM5 dimer (Goldstone et al., 2014; Sanchez et al., 2014). Thus, RING domains from multiple different TRIM5 dimers apparently must come together to transfer ubiquitin. Our lattice structures reveal such associations of three TRIM5 RING domains at local three-fold axes in the hexagonal net (Figure 7D). This suggests that two of the RING domains may join to form an active dimer and that the third “orphan" RING domain could then be used as a substrate for autoubiquitylation. This idea is supported by 1) recent studies that demonstrate that autoubiquitylation occurs *in vitro* and in cells and that Lys45 and Lys50 within the RING domain of rhesus TRIM5α are preferentially ubiquitylated (Fletcher et al., 2015), and 2) by the accompanying structural studies (Wagner et al., 2016) of a truncated rhesus TRIM5α protein comprising a B-box 2 and the truncated coiled-coil and L2 linker domains (termed “mini-TRIM”) which reveal that the B-box 2 domains can mediate trimerization (Wagner et al., 2016). Hence, in

addition to enhancing binding avidity, formation of hexagonal TRIM5 lattices may also activate the ubiquitin signaling cascade that ultimately results in capsid dissociation and inhibition of reverse transcription.

MATERIALS AND METHODS

Plasmids, cells and antibodies

HEK 293T and HeLa-M cells were grown at 37°C with 5% CO_2 in DMEM media (Gibco) supplemented with 10% heat-inactivated FCS and 2 mM L-Glutamine. Plasmid constructs for virus production and for expressing TRIM5, CA, and OSF-CypA in mammalian, insect and bacterial cells were created by standard cloning and mutagenesis methods (details available upon request). The plasmids used in this study are summarized in Supplementary file 1A. All plasmids have been submitted to the Addgene (https://www.addgene.org/) and DNASU (https://dnasu.org/DNASU/) public repository.

TRIM5-21R electron cryo-tomography (ECT)

TRIM5-21R and TRIM5-21R$_{\Delta SPRY}$ proteins were expressed, purified and assembled into 2D crystals as previously described (Ganser-Pornillos et al., 2011), except that the TRIM5-21R$_{1-300}$ assembly was promoted by addition of an equal volume of 0.1 M Sodium chloride, 0.1 M Bicine pH 9.0, 20% PEG MME to the concentrated protein solution.

To prepare samples for ECT, 3 µl of polymerized lattice was mixed with 10 nm Au fiducials and applied to a 2/2 holey carbon-coated Cu EM grid (Quantifoil) and transferred with forceps to the environment chamber of a Vitrobot Mark III (FEI) maintained at 25 °C and 80% relative humidity. Excess liquid was manually blotted from the grids on one side before plunging into liquid ethane. Cryo-preserved grids were imaged in a 300-kV FEI G2 Polara equipped with a field emission gun and energy filter

583 (slit width set at 20 eV), and fitted with a K2 Summit direct detector. Tilt-series were
584 collected over a series of angles ranging from -60° to +60° using a step size of 1°;
585 22,500x magnification (effective pixel size of raw data is 5 Å), a total dose of 150 e/Å^2,
586 and a defocus of -6 μm. UCSF Tomo (Zheng et al., 2007) was used to collect the tilt
587 series and 3D reconstructions were carried out using a weighted back-projection
588 algorithm tracking 10 nm fiducials in IMOD (Kremer et al., 1996a). Pixel size in the final
589 reconstruction was 20 Å.

590 Subtomogram averages of the TRIM5-21R and TRIM5-21R$_{\Delta SPRY}$ lattices were
591 generated using PEET in IMOD (Nicastro et al., 2006). 153 and 75 vertices were
592 selected in the TRIM5-21R and TRIM5-21R$_{\Delta SPRY}$ 2D lattices, respectively, and a volume
593 of 60 nm x 60 nm x 20 nm (x,y,z) centered on the refined positions of the selected
594 vertices was used to generate the averaged volume. To localize the SPRY domain in
595 the full-length TRIM5-21R lattice, the density values of the averaged lattice volumes
596 were rescaled to reflect a mean value of zero and standard deviation of 10. The
597 volumes were then aligned in Chimera (Pettersen et al., 2004) and the TRIM5-21R$_{\Delta SPRY}$
598 density values were subtracted from the TRIM5-21R volume. The resulting density
599 difference map was contoured and displayed at 3 sigma above the mean.

600 An important difference between the TRIM5-21R and TRIM5-21R$_{\Delta SPRY}$
601 assemblies is that in the absence of the SPRY domains, multiple hexagonal lattices
602 stacked on "top" of one another close together, laterally offset by a quarter, half, or
603 three-quarters the distance across a hexagon. Thus in projections through 3-D sub-
604 tomogram averages, like those shown in the bottom middle panels of 1C and D, all of
605 these other offset lattices appear, but less prominently than the main lattice. Due to the

special pattern of the offsets (one quarter, half, and three-quarters across) and the hexagonal geometry, their projections all intersect at the center of the arms of the main lattice, causing that position to appear especially dark and large. Furthermore, the four-helix bundle of both TRIM5-21R and TRIM5-21R$_{\Delta SPRY}$ also contributed to the observed densities in the center of the hexagon edges. Figure 1E shows, however, a thin slice through the 3-D difference map containing only the main hexagonal lattice, revealing the position of the SPRY domain without interference from the lattices above and below.

To quantify the variability in the TRIM5-21R hexagonal lattice, the refined positions of each vertex were used to calculate: 1) the distance between neighboring vertices, and 2) the average angle of hexamer edges extending from the three-fold vertices. These values were entered into the *imodsetvalues* program in IMOD and a pseudo-colored model was generated to reflect length (colored lines) and average angles (colored spheres) (Figure 1F).

TRIM5 restriction assays

HEK 293T cells were used to generate lentiviral vectors for transduction of HeLa cells for expression of TRIM5 proteins with a C-terminal Flag One-Strep tag. pCMV-ΔR8.2 (structural genes), pCMV-VSVG (envelope), and CSII-IDR2 (contains a packaging signal and genes for TRIM5 and DsRed) were co-transfected in 293T cells. After 3 days, virion-containing media was removed from the cells, passed through a 0.45 μm filter (Nalgene SFCA syringe filters), layered on top of a 20% sucrose cushion in HS buffer (10 mM HEPES pH 7.2 and 140 mM NaCl) and spun in an Optima L-90K Ultracentrifuge at 96,281 g (Beckman SW32 Ti rotor) for 2 hours at 4°C. Virion-

containing pellets were resuspended in HS buffer, aliquoted, and frozen at -80°C. Thawed aliquots were titrated on HeLa cells to determine viral titers by monitoring the number of DsRed positive cells using fluorescence-activated cell sorting (FACS).

HeLa cells (1 x 10^5 cells per well of 6-well plate) were transduced with lentiviral vectors expressing different TRIM5 proteins at an MOI of 1. Three days after transduction, cells were split and reseeded at 5 x 10^4 cells per well of a 24-well plate and infected with increasing amounts of HIV-GFP per well. The remaining cells were used for western blot analysis to determine TRIM5 expression levels. Three days after infection with HIV-GFP, cells were trypsinized and GFP and DsRed positive cells were counted using FACS. Only DsRed positive cells (which also expressed TRIM5) were used for statistical analysis of HIV-GFP restriction.

Expression and purification of native TRIM5 proteins

Recombinant baculoviruses expressing TRIM5 proteins with either N-terminal One-STrEP-FLAG (OSF) or C-terminal FLAG-One-STrEP (FOS) PreScission protease-cleavable tags were generated using the Bac-to-Bac baculovirus expression system (Life Technologies). Suspension SF9 insect cells (2 L at 2 x 10^6 cells/ml) grown in ESF-921 medium (Expression Systems) were infected with recombinant baculoviruses at multiplicities of infection of 10, and harvested by centrifugation 48 hours later. All purification steps were performed at 4°C. Cell pellets were resuspended in 5 times the pellet volume of lysis buffer (70 mM N-Cyclohexyl-2-aminoethanesulfonic acid (CHES), 100 mM NDSB-256, 1.5% Triton X-100, 100 nM $ZnCl_2$, 1 mM Tris(2-carboxyethyl)phosphine (TCEP), 0.7% protease inhibitor cocktail (v/v, Sigma), 100 U

avidin, pH 10) and lysed by freeze-thaw and sonication (3 x 30 seconds on ice; Branson sonifier 450, 50% duty cycle, 50% output). Cell lysates were clarified by ultracentrifugation at 184,000 g (Beckman Ti 50.2 rotor) for 1 hour. The supernatants were filtered (0.45 µm) and loaded onto a 5 ml StrepTrap HP column (GE Healthcare) pre-equilibrated in binding buffer (20 mM CHES, 100 nM $ZnCl_2$, 1 mM TCEP, pH 10). The column was washed with 20 column volumes (CV) of binding buffer supplemented with 1 M NaCl and 100 U avidin (VWR), followed by 5 CV of binding buffer. The protein was eluted in 6 CV binding buffer supplemented with 2.5 mM D-desthiobiotin (Sigma). The eluate was diluted to 0.3 mg/ml protein in binding buffer to minimize protein loss due to self-assembly, and dialyzed overnight against 1L cleavage buffer (25 mM Tris, 1 mM TCEP, pH 8) supplemented with ~ 1:100 (by mass, enzyme:substrate) His_6-HRV14-3C and His_6-Usp2 enzymes to remove the OSF tag and any linked ubiquitin added during insect cell expression. TRIM5α_{hu} and TRIMCyp formed soluble/insoluble aggregates at pH 8 and were therefore dialyzed against 20 mM CHES, 1 mM TCEP, pH 9. Most TRIM5 proteins were sensitive to non-specific internal proteolysis by HRV14-3C protease. We therefore used the minimal amount (which differed between constructs) required to completely cleave the OSF tag overnight. When cleavage was complete, the pH of protein solution was adjusted to 10 by direct addition of 1 M CHES, pH 10, to a final concentration of 100 mM. The sample was applied onto two tandem 5 ml HiTrap Q HP columns (GE Healthcare) pre-equilibrated with binding buffer, and eluted with a 12 CV linear NaCl gradient (0-1 M) in binding buffer. Fractions containing TRIM5 proteins were pooled, dialyzed against 1 L binding buffer for at least 4 hours, loaded onto a HiLoad 16/600 Superdex 200 gel filtration column (GE Healthcare) pre-equilibrated with

675 binding buffer, and eluted in 1 CV of binding buffer. Fractions corresponding to TRIM5
676 dimers were pooled and concentrated to 1 mg/ml using a Vivaspin 20 concentrator
677 (10,000 MWCO PES for TRIM5α$_{AGMpyg}$ ΔSPRY and 30,000 MWCO PES for full-length
678 TRIM5α and TRIMCyp, Sartorius Stedim). Average yields were 4 mg (1.3-9.6 mg) per
679 1L insect cell culture and protein identities were confirmed by electrospray ionization
680 mass spectrometry (see Supplementary file 1B).
681
682 **TRIM5 2D crystallization**
683 Freshly purified TRIM5α$_{AGMpyg}$ protein was concentrated to 1-3 mg/ml and assembled by
684 incubating at 23°C for 1 hour and then at 4°C for 1-2 days. For EM analyses, 5 µl
685 sample aliquots were incubated on carbon-coated EM grids for 5 minutes. The grids
686 were washed by placing each grid on a single 40 µL drop of 0.1 M KCl for 3 minutes,
687 briefly blotted, and then stained on a single 20 µL drop of 2% uranyl acetate for an
688 additional 3 minutes.
689 Unlike TRIM5α$_{AGMpyg}$, TRIMCyp did not spontaneously assemble into hexagonal
690 lattices following concentration. However, crystals were occasionally observed when an
691 equal volume of 0.01 M Cobalt chloride hexahydrate, 0.1 M MES monohydrate pH 6.5,
692 and 1.8 M Ammonium sulfate was added to freshly concentrated protein at ~1 mg/ml.
693
694 **Templated assembly of TRIM5 on hexagonal arrays of HIV-1 CA-NC**
695 As previously described (Ganser-Pornillos et al., 2011), 2-dimensional crystals
696 composed of cross-linked, hexagonal HIV-1 CA were prepared by incubating 232 µM
697 CA-NC$_{A14C/E45C/W184A}$ with a small 25-TG oligo (143 µM). TRIM5 proteins were then

added in 1- to 10-fold molar excess, and the pH was immediately adjusted to 9 by direct addition of Tris buffer to a final concentration of 100 mM. Samples were incubated for 1-96 hours, applied to carbon-coated EM grids for 60 seconds, washed and stained as described above, and visualized by EM. 10-fold lower amounts were sufficient for TRIMCyp$_{K283D,Q287D}$ templated assembly.

Bacterial protein expression and purification

HIV-1 CA$_{A14C/E45C/A92E}$

2 liters of *E.coli* Rosetta (λDE3) pLysS cells (Stratagene) carrying the HIV-1 CA A14C/E45C/A92E expression construct were grown to an $OD_{600\ nm}$ of 0.6 in LB medium at 37°C, cooled to 19°C and protein expression was induced with 1 mM isopropyl-β-D-thiogalactopyranoside (IPTG) followed by overnight incubation with shaking. HIV-1 CA proteins were purified and assembled into tubes as previously described (Pornillos et al., 2010), except that a higher concentration of DTT (100 mM) was used during protein purification to improve solubility and increase yields. All purification steps were performed at 4°C. Cells were lysed as described above and proteins were purified from clarified lysates by ammonium sulfate precipitation, dialyzed against 25 mM MOPS, 100 mM DTT, pH 6.5, and loaded onto a 5 ml HiTrap Q HP column (GE Healthcare) pre-equilibrated with the same buffer. The flow-through was applied onto a 5 ml Hi-Load SP Sepharose High Performance column (GE Lifesciences) and eluted with a linear NaCl gradient (0-500 mM) in the same buffer. Fractions containing CA proteins were pooled and dialyzed overnight against storage buffer (20 mM Tris, 40 mM NaCl and 100 mM DTT, pH 8). The CA proteins were then concentrated to a stock of 3 mg/ml using a

721 Vivaspin 20 concentrator (10,000 MWCO PES, Sartorius Stedim) and stored at -80°C.
722 Yields were ~20 mg per 1L of culture and the protein identity was confirmed by ESI-MS
723 (MW_{exp}=25,667 Da, MW_{calc}=25,667 Da).
724 *OSF-Cyclophilin A (OSF-CypA)*
725 OSF-CypA was expressed in 2 liters of *E. coli* Rosetta (λDE3) pLysS cells
726 (Stratagene) grown in ZYP-5052 media using an autoinduction system (Studier, 2005).
727 Cells were lysed on ice by sonication in lysis buffer (50 mM Tris, pH 8, 50 mM NaCl, 10
728 mM β-mercaptoethanol (β-ME), 0.2% (w/v) deoxycholate, 2.5 nmol avidin, 20 µg/ml
729 DNAse) supplemented with protease inhibitors (20 µg/ml PMSF, 0.4 µg/ml pepstatin,
730 0.8 µg/ml leupeptin and 1.6 µg/ml aprotinin). All purification steps were performed at
731 4°C. Cell lysates were clarified by centrifugation at 17,649 g (Beckman JA-20 rotor) for
732 45 minutes, filtered (0.45 µm) and loaded onto two 5 ml tandem StrepTrap HP columns
733 (GE Healthcare) pre-equilibrated in binding buffer (100 mM Tris, 150 mM NaCl, 10 mM
734 β-ME, pH 8). The column was washed with 10 CV of binding buffer and OSF-CypA was
735 eluted in 3CV of the same buffer supplemented with 2.5mM D-desthiobiotin. The protein
736 was dialyzed against Q buffer (50 mM Tris, 50 mM NaCl, 10 mM β-ME, pH 8) and
737 loaded onto two connected 5 ml HiTrap HP Q-Sepharose anion exchange columns (GE
738 Healthcare) pre-equilbrated in the same buffer. The OSF-CypA-containing flowthrough
739 was collected and concentrated using Amicon Stirred Ultrafiltration Cells (Millipore).
740 OSF-CypA (>99% pure) was obtained in high yields (～100 mg per 1L bacterial culture)
741 and its identity was confirmed by ESI-MS (MW_{exp} =23,806 Da, $MW_{calc, -Met1}$=23,807 Da).
742
743 **Assembly of hyperstable $CA_{A14C/E45C/A92E}$ tubes**

744 $CA_{A14C/E45C/A92E}$ tubes were assembled at 1 mg/ml by dialysis against dialysis
745 buffer (20 mM Tris pH 8.0, 1 M NaCl, and 100 mM DTT) at 4°C overnight, followed by
746 dialysis against the same buffer lacking DTT overnight to allow the formation of disulfide
747 crosslinks within the CA hexamers. Disulfide-crosslinked CA tubes were then dialyzed
748 against 20 mM Tris, 40 mM NaCl, pH 8.0 and stored at 4°C.
749
750 **TRIM5-CA tube binding experiments**
751 TRIM5-CA tube binding experiments were performed as previously described,
752 with minor modifications (Ganser-Pornillos et al., 2011; Langelier et al., 2008; Stremlau
753 et al., 2006). Recombinant TRIM5α and TRIMCyp proteins (0.25 μM) were incubated
754 alone or with $CA_{A14C/E45C/A92E}$ tubes (2 μM) in binding buffer (20 mM HEPES, 25 mM
755 NaCl, 1 mM TCEP, pH 7.2) in a final volume of 225 μl at 4 °C for 1 hour. Aliquots (10 μl)
756 of the incubation mixtures were mixed with 2X SDS-PAGE sample loading buffer for
757 assessment of protein amounts in the inputs. Aliquots (200 μl) of the mixtures were
758 layered onto a 60% (w/v) sucrose/PBS cushion (4 ml, prepared in binding buffer lacking
759 TCEP) and centrifuged at 108,109 g (Beckman SW50.1 rotor) for 30 minutes at 4°C to
760 separate free TRIM5α or TRIMCyp and unassembled CA proteins from CA tube-bound
761 TRIM5 proteins and pelletable CA tubes. Following centrifugation, aliquots (45 μl) of
762 supernatant (500 μl in total) were mixed with 4X SDS-PAGE sample loading buffer, and
763 the pellets were resuspended in 25 μl 1X SDS-PAGE sample loading buffer. The TRIM5
764 and CA proteins in the input (3%), supernatant (3%) and pellet (30%) were separated
765 by 12% SDS-PAGE and analyzed by western blotting as described above.
766

Negative stain transmission electron microscopy

3.5 µl sample solutions of undecorated or TRIM5-decorated CA tubes were spread onto the carbon side of freshly glow-discharged Formvar carbon-coated 200-mesh copper grids (Electron Microscopy Science). The samples were incubated for 4 minutes, rinsed briefly by flotation on a drop of 100 mM KCl, blotted dry, stained for 2 minutes in filtered, saturated uranyl acetate (or 1 minute of phosphotungstate), blotted dry, and allowed to air dry. Samples were viewed on a JEOL JEM-1400 Plus transmission electron microscope operated at 120 kV accelerating voltage, and images were acquired as Gatan Digital Micrograph 3 (DM3) files with a Gatan Ultrascan CCD camera or on a Hitachi 7100 TEM at 75 kV accelerating voltage with a Gatan ORIUS CCD camera, and converted into JPEG images using ImageJ software (NIH Bethesda, MD, USA).

Screening for TRIM5 decoration of CA tubes

TRIM5-CA tube complexes were prepared by incubating TRIM5α or TRIMCyp$_{K283D,\ Q287D}$ proteins with hyperstable CA tubes in 50 mM Tris, 8 mM NaCl buffer at 4°C. Decoration conditions were surveyed at a constant CA concentration (7.5 µM) over a range of TRIM5 concentrations (0.5-22.5 µM, corresponding to molar ratios of TRIM5 to CA of 1:16, 1:8, 1:6, 1:3, 1:1 and 3:1), pH values (8.0 and 9.0) and incubation times (4-92 hours). Conditions that produced the best TRIM5 decoration and minimal CA-free TRIM5 self-assemblies were determined by negative stain TEM imaging on a JEOL JEM-1400 Plus transmission electron microscope as described above. Image contrast was uniformly adjusted to enhance the decoration patterns of

TRIM5 proteins on CA tubes using Adobe Photoshop CS5. The spacings of hexagonal TRIM5 rings were measured using ImageJ. Human TRIM5α and TRIM5α_{R332P} tended to aggregate in all incubation conditions tested. These aggregates sometimes associated with CA tubes, but could be readily distinguished from ring-like decorated tubes. For scoring, images were judged blind by two independent colleagues.

Deep-etch electron microscopy

TRIM5α-CA tube complexes were prepared by incubating 1 μM TRIM5α_{AGMpyg} proteins with 8 μM hyperstable CA tubes in 50 mM Tris, pH8, and 8.2 mM NaCl buffer at 4°C for 32 hours. Quick-freeze deep-etch EM was performed according to published protocols (Heuser, 1980). Briefly, a 3 μl droplet of TRIM5α_{AGMpyg} decorated tubes was placed onto an acid cleaned, air dried 3x3 mm coverglass and covered by a 0.05 mm thick, 3 mm diameter wafer of sapphire on top. The sample was then mounted onto the freezing stage of a Heuser designed “Slam Freezer” and frozen by forceful impact against a pure copper block, cooled to 4°K with liquid helium. Frozen samples were transferred to a liquid nitrogen cooled Balzers 400 vacuum evaporator. Freeze fracture occurred by popping off the sapphire top at -104°C under vacuum. Samples were etched for 210 seconds at -104°C and rotary replicated with ~ 3 nm platinum deposited from a 15° angle above the horizontal, followed by an immediate ~10 nm stabilization film of pure carbon deposited from an 85° angle. Replicas were floated onto a dish of concentrated hydrofluoric acid and transferred through 3 rinses of dH_2O containing a loopful of Photo-flo. Replicas were picked up on formvar coated copper grids, and imaged on a JEOL 1400 microscope with attached AMT digital camera.

Co-assembly of TRIM5α and HIV-1 CA

Coassembly experiments were performed by incubating HIV-1 CA (650 μM) alone or with $TRIM5\alpha_{AGMpyg}$ (1-15 μM) in assembly buffer (20 mM Tris, pH8, 50 mM NaCl) at 37°C for 2-3 hours, followed by a 2 hour incubation at room temperature. Following incubation, a 3.5 μL aliquot of the assembly reaction was incubated on carbon-coated EM grids (Electron Microscopy Science) for 1-2 minutes. Grids were then placed directly onto a 20 μL drop of 0.1 M KCl for 2 min, blotted and moved to a 20 μL drop of 2% uranyl acetate for 2 minutes, blotted, and air dried. Samples were imaged on either a Tecnai T12 or a Tecnai F20 microsope operating at 120 kV.

Preparation of HIV-1 virions

HEK 293T cells (29 x 10 cm plates) were co-transfected (polyethylenimine, PEI, Polysciences) at 70-80% confluency with pLOX-GFP (5 μg DNA/plate) (Salmon et al., 2000) and pCMV-ΔR8.2 vectors (5 μg DNA/plate) (Naldini et al., 1996) that expressed HIV structural proteins encoding wild type or mutant CA sequences (A14C/E45C or A14C/E45C/A92E). 40 hours later, virion-containing media was pooled, filtered (0.45 μm) and pelleted by ultracentrifugation through a 4 ml, 20% sucrose/PBS cushion in 25x89 mm polyallomer centrifuge tubes (Beckman Coulter) at 96,281 g (Beckman SW32 Ti rotor) for 2 hours at 4°C. Subsequent core purification steps were performed at 4°C.

Sucrose gradient purification of HIV-1 cores

Wild type and hyperstable HIV-1 A14C/E45C cores were isolated from virions using an adaptation of a sucrose gradient spin-through method (Kotov et al., 1999; Langelier et al., 2008). Virion pellets were resuspended with 2.4 ml ST buffer (20 mM Tris, 75 mM NaCl, pH 7.4). 6 x 11.5 ml 30-70% (w/v) continuous sucrose gradients in ST buffer were made in 14x89 mm polyallomer centrifuge tubes (Beckman Coulter) using a gradient maker (Biocomp). The gradients were overlaid with a 300 µl 15% (w/v) sucrose cushion in ST buffer containing 0.5% Triton X-100 (to delipidate the virions as they migrated through the cushion) and then with a 300 µl non-detergent barrier layer (7.5% sucrose in ST buffer), which protected virions from premature detergent exposure. Concentrated virions were applied to the top of the gradient and centrifuged through the cushion and gradient at 151,263 g (Beckman SW41 Ti rotor) for 16 hours. Twelve 1 ml fractions were collected from the bottom of each tube and the density of each fraction was determined from the refractive index using a digital refractometer (Leica). The CA content in each fraction was analyzed by western blotting using rabbit anti-HIV-1 CA polyclonal antibodies (made in-house, UT 416, 1:3000 dilution). Fractions 10-12 (density = 1.22-1.27 g/ml), which contained intact HIV-1 cores were pooled, diluted with ST buffer, and subjected to ultracentrifugation at 151,263 g (Beckman SW41 Ti rotor) for 2 hours. The pelleted cores were resuspended in 240 µl ST buffer and recovered yields were quantified as described below.

Affinity purification of HIV-1 cores

2.4 ml of concentrated virions in PBS were mixed gently with an equal volume of lysis buffer (1% Triton X-100, 100 mM Tris, 2M NaCl, pH 8) in the presence of 35 µM

OSF-CypA and incubated for 3 minutes at 23°C. Subsequent core purification steps were performed at 4°C. 8 mg of MagStrep”type2HC” beads (IBA GmbH) were added to the lysed virions and mixed gently by inversion for 7 min to allow OSF-CypA to bind the membrane-stripped cores. The sample was then placed on a PolyATtract system 1000 magnet separation stand (Promega) for 3 min, and the supernatant (‘Flow-through’ in Figure 5 – figure supplement 1E) was removed. Captured cores were washed 10 times with high salt buffer (50 mM Tris, 1 M NaCl, pH 8) to remove unbound CA proteins and contaminating vesicles and the final wash sample was saved for western blot analysis (‘Wash’ in Figure 5 – figure supplement 1E). Cores were eluted in 150 µl elution buffer (50 mM Tris, 75 mM NaCl, pH 8) supplemented with 40 µM Cyclosporine A (Sigma-Aldrich) buffer and incubated with inversion for 40 min. The sample was briefly centrifuged in a tabletop ultracentrifuge at 1,000 g for 5 seconds and placed on a Magnesphere Technology Magnetic Separation Stand (Promega) for 5 minutes. The supernatant containing the purified cores (‘Eluate’ in Figure 5 – figure supplement 1E) was collected and used in the experiments shown in Figures 5, 6, 7, Figure 5 – figure supplement 1, and Figure 7 – figure supplement 1, 2, and 3. Beads before and after CsA elution were also saved for western blot analyses (Figure 5 – figure supplement 1E).

Characterization of purified hyperstable cores

Core yields

Virion inputs and core yields were quantified by western blot densitometry against a standard curve of recombinant CA proteins for reference. The recovery of

cores from virions was calculated by normalizing core yields of CA to corresponding virion CA inputs, which were set to 100%. As illustrated in Figure 5, disulfide crosslinks apparently stabilized the HIV-1 cores, resulting in a ~4 fold increase in the core recovery (0.8±1%; core yields: 0.6±0.5 μg CA; virus inputs: 100±80 μg CA, n=10) compared to wild type cores (0.2±0.1%; core yields: 0.08±0.05 μg CA; virus inputs: 40±30 μg CA, n=7). The affinity purification method consistently raised the yield of hyperstable HIV-1 A14C/E45C cores by an additional ~4 fold (3±2%; core yields: 1±0.6 μg CA; virus input: 40±8 μg CA, n=3) vs. the sucrose gradient spin-through method. Core recovery was not affected by the A92E mutation (3±1%; core yields: 3±1 μg CA; virus inputs: 100±60 μg CA, n=7).

Analyses of HIV-1 core morphologies

Discrete particles were imaged by negative stain EM and scored as “tubular” if their edges appeared parallel, as “spherical” if they were spherical or elliptical, and as “conical” if they lacked the above properties. The final class included conical, triangular, bullet-shaped, and coffin-shaped cores.

Disulfide crosslinks

To examine disulfide crosslinking within purified cores, sucrose gradient fractions 7-9 and 10-12 were pooled separately, mixed with SDS-PAGE sample loading buffer lacking β-ME (or containing the concentrations designated in Figure 5C), treated with 31.25 μM methyl methanethiosulfonate (Pierce Biotechnology), heated at 95°C for 10 min, and electrophoresed on 4-15% gradient SDS polyacrylamide gels (Bio-Rad) and analyzed by western blotting.

Analyses of HIV-1 core protein components

905 Purified cores were denatured in SDS-PAGE sample loading buffer, resolved on
906 4-15% gradient SDS polyacrylamide gels (Bio-Rad) and stained using SilverQuest^{TM}
907 silver staining kit (invitrogen).
908
909 **TRIM5-core binding experiments**
910 Recombinant TRIM5α$_{AGMpyg}$ (0.5 μM) and TRIM5α$_{cpz}$ (0.5 μM) proteins were
911 incubated at 4 °C for 1 hour alone or with hyperstable HIV-1 cores (0.5-1 μM) in binding
912 buffer (40 mM HEPES, 50 mM NaCl, 1 mM TCEP, pH 7.2) in a final volume of 75 μl.
913 Rhesus TRIM5α$_{rh}$ (0.25 μM) was incubated alone or with hyperstable cores under
914 slightly more alkaline conditions (40 mM Tris, 50 mM NaCl, 1 mM TCEP, pH 8) to
915 minimize untemplated assembly of TRIM5α during sedimentation. Human TRIM5α
916 proteins were not used in these assays because they tended to aggregate and pellet,
917 even in the absence of HIV-1 cores. TRIMCyp was also not used owing to low levels of
918 residual cyclosporine A in the core preparations. Aliquots (5 μl) of the mixtures were
919 mixed with 2X SDS-PAGE sample loading buffer ('Input' in Figure 6). The mixtures were
920 layered onto a 30% (w/v) sucrose/PBS cushion (4 ml, prepared in binding buffer lacking
921 TCEP) and centrifuged at 149,632 g (Beckman SW50.1 rotor) for 2.5 hours to separate
922 free TRIM5α and unassembled CA proteins from capsid-bound TRIM5 proteins and
923 pelletable cores. Following centrifugation, aliquots (45 μl) of supernatant (500 μl in total)
924 were mixed with 4X SDS-PAGE sample loading buffer, and the pellets were
925 resuspended in 25 μl 1X SDS-PAGE sample loading buffer. The TRIM5 and CA
926 proteins in the input (2%), supernatant (2%) and pellet (30%) were separated by 12%
927 SDS-PAGE, electrophoretically transferred onto nitrocellulose membranes (Bio-Rad)

928 and analyzed by western blotting with mouse anti-TRIM5α monoclonal (clone 5D5-1-1,
929 NIH AIDS Research and Reference Reagent Program, 1:1000 dilution) and rabbit anti-
930 HIV-1 CA polyclonal (made in-house, UT 416, 1:3000 dilution) antibodies. Secondary
931 IRDye800cw-conjugated Donkey anti-mouse IgG (1:10,000, Rockland) or IRDye700DX-
932 conjugated Donkey anti-rabbit IgG (1:10,000, Rockland) antibodies were visualized
933 using an Odyssey infrared imaging system (LI-COR Bioscience). The integrated
934 intensities of protein bands on the western blots were measured using the Odyssey
935 software (LI-COR Bioscience). The molar ratios of TRIM5α_{AGMpyg} to CA in the pellets
936 were estimated from standard curves constructed from known amounts of
937 TRIM5α_{AGMpyg} and CA loaded on the same gel.
938
939 **Screening for TRIM5 decoration of HIV-1 cores**
940 TRIM5α-core complexes were prepared by incubating TRIM5α_{rh} with affinity-
941 purified hyperstable HIV-1 cores in 50 mM HEPES (pH 8.0) or CHES (pH 9.0), 0.1 mM
942 TCEP buffer at 4°C. Decoration conditions were surveyed over a range of TRIM5α_{rh}
943 concentrations (0.25-2 μM), NaCl concentrations (50 or 200 mM), and incubation times
944 (2-92 hours). Conditions that gave the best TRIM5 decoration on HIV-1 cores with
945 minimal TRIM5 self-assemblies were determined by negative stain TEM with imaging
946 on a JEOL JEM-1400 Plus transmission electron microscope as described above. Clear
947 decoration was difficult to discern in the majority of the TRIM-incubated cores, likely
948 because TRIM decorations were obscured by uranyl acetate staining of the underlying
949 viral ribonucleoprotein complexes, and cores with clear external TRIM5 decoration
950 patterns were observed on only ~5% of 907 core particles examined. Cores incubated

in the absence of TRIM proteins and stained under the same conditions did not ever show equivalent decorations.

ECT of TRIM5α-decorated HIV-1 cores and tubes

Cryo-grid preparation

TRIM5α-decorated CA tubes were made by incubating 1.5 μM TRIM5α_{AGMpyg} with 695 μM wild type CA in 90 μl of assembly buffer (20 mM HEPES, 50 mM NaCl, pH 8) at 37°C for 2 hours, followed by a 2 hour incubation at room temperature. TRIM5α-decorated HIV-1 cores were made by incubating 0.5 μM TRIM5α_{AGMpyg} with 0.6 μM CA equivalents of hyperstable HIV-1 cores in 75 μl of binding buffer (40 mM HEPES, 50 mM NaCl, 1 mM TCEP, pH 7.2) at 4°C for 1 hour, a condition that produced saturation binding in the co-sedimentation assay (data not shown). TRIM5α-tube complexes, cores, or TRIM5α-core complexes were mixed with BSA-coated colloidal gold particles (10 nm, SPI Supplies), which served as fiducials required for aligning the tilt stacked images. For crosslinked complexes, the pH of samples was adjusted to 8 by adding 1/20th the sample volume of 1 M HEPES, pH 8, and the samples were incubated with 1 mM Sulfo-EGS (Pierce Biotechnology) at 23°C for 10 minutes in 88 μl total reaction volume. The cross-linking reaction was quenched by direct addition of 1 M Tris, pH 7.4, to a final concentration of 50 mM, followed by 15 minute incubation at 23°C. This treatment crosslinked ~87% and ~76% of the TRIM5α_{AGMpyg} and CA subunits of TRIM5-core complexes, respectively, as analyzed by SDS-PAGE and western blotting (data not shown). Samples (3.5 μl) were placed on the carbon side of freshly glow-discharged Quantifoil R2/2, 300 mesh holey carbon grids (SPI Supplies) for 1 min, thinned by

automatic blotting using FEI Vitrobot (-1.5 mm offset, 6-8 seconds, with filter papers from both sides at 80-85% relative humidity) and vitrified by plunge-freezing into liquid ethane. The cryo-grid was transferred to the microscope using a cryo-transfer holder.

ECT

Images were collected using a FEI Polara 300kV FEG transmission electron microscope equipped with an energy filter (slit width 20 eV; Gatan) and a 4k x 4k K2 Summit using the direct electron counting mode (Gatan). Pixels on the detector represented 0.26 nm (41,000x) at the specimen level. The tilt series were recorded from -60° to +60° with an increment of 1° and 4 μm underfocus. The cumulative dose of a tilt-series was 80-100 e-/Å^2. UCSF Tomo (Zheng et al., 2007) was used for automatic acquisition of the tilt series and 2D projection images. The tilt series was aligned and binned by 4 into 1k x 1k using the IMOD software package (Kremer et al., 1996a) and 3D reconstructions were calculated using the simultaneous reconstruction technique (SIRT) using the TOMO3D software package (Agulleiro and Fernandez, 2011), or weighted back projection using IMOD. Noise reduction was performed using the non-linear anisotropic diffusion (NAD) method in IMOD (Kremer et al., 1996b), typically using a K value of 0.03 – 0.04 with 10 iterations.

Segmentation and isosurface generation

Segmentation and isosurface rendering was performed in Amira (FEI). The outer boundary of the HIV-1 tube or core was first manually identified and a material mask was generated inside the boundary. A second region of interest surrounding the tube or core that typically extended 9 nm from the exterior surface was generated (densities inside this region correspond to TRIM5α protein). The area inside the second region

was segmented and an isosurface generated for the densities inside. Islands containing six voxels or less in 3D were deleted for the segmented cores and four voxels or less were deleted for the co-assembled tube. The exterior layer of capsid protein within the HIV-1 tube or core of the first material was also segmented using a similar threshold value and an isosurface was generated. Movie image sequences were generated in .jpg format in Amira (FEI) and converted into movies using QuickTime Player 7. Photoshop CS6 (Adobe) was then used to produce the finalized versions of the movies.

Fitting the TRIM5 structural model to the cryoEM map

Crystal structures of the B-box 2 trimer (PDB 5EIA; Wagner et al. 2016) and B-box 2/coiled-coil dimer (PDB 4TN3, Goldstone et al., 2014) were fitted manually as separate units into the map using UCSF chimera (Pettersen et al., 2004). The trimer structures were initially placed at putative three-fold densities, and then iterative superpositions and manual adjustments were performed to optimize the overlap between the B-box 2 portions of the two source PDB files. No geometric optimization was performed, and the fitting should be treated as a simple proof of principle that the dimensions of the hexagon densities observed in the cryotomograms are compatible with dimensions and interactions observed in the crystal structures.

REFERENCES

Agulleiro, J.I., and Fernandez, J.J. (2011). Fast tomographic reconstruction on multicore computers. Bioinformatics *27*, 582-583.

Altfeld, M., and Gale, M., Jr. (2015). Innate immunity against HIV-1 infection. Nature immunology *16*, 554-562.

Anderson, J.L., Campbell, E.M., Wu, X., Vandegraaff, N., Engelman, A., and Hope, T.J. (2006). Proteasome inhibition reveals that a functional preintegration complex intermediate can be generated during restriction by diverse TRIM5 proteins. J Virol *80*, 9754-9760.

Benjamin, J., Ganser-Pornillos, B.K., Tivol, W.F., Sundquist, W.I., and Jensen, G.J. (2005). Three-dimensional structure of HIV-1 virus-like particles by electron cryotomography. J Mol Biol *346*, 577-588.

Berthet-Colominas, C., Monaco, S., Novelli, A., Sibai, G., Mallet, F., and Cusack, S. (1999). Head-to-tail dimers and interdomain flexibility revealed by the crystal structure of HIV-1 capsid protein (p24) complexed with a monoclonal antibody Fab. EMBO J *18*, 1124-1136.

Bhattacharya, A., Alam, S.L., Fricke, T., Zadrozny, K., Sedzicki, J., Taylor, A.B., Demeler, B., Pornillos, O., Ganser-Pornillos, B.K., Diaz-Griffero, F.*, et al.* (2014). Structural basis of HIV-1 capsid recognition by PF74 and CPSF6. Proc Natl Acad Sci USA *111*, 18625-18630.

Bichel, K., Price, A.J., Schaller, T., Towers, G.J., Freund, S.M., and James, L.C. (2013). HIV-1 capsid undergoes coupled binding and isomerization by the nuclear pore protein NUP358. Retrovirology *10*, 81.

Bieniasz, P.D. (2003). Restriction factors: a defense against retroviral infection. Trends Microbiol *11*, 286-291.

Bieniasz, P.D. (2004). Intrinsic immunity: a front-line defense against viral attack. Nature immunology *5*, 1109-1115.

Biris, N., Tomashevski, A., Bhattacharya, A., Diaz-Griffero, F., and Ivanov, D.N. (2013). Rhesus monkey TRIM5alpha SPRY domain recognizes multiple epitopes that span several capsid monomers on the surface of the HIV-1 mature viral core. J Mol Biol *425*, 5032-5044.

Biris, N., Yang, Y., Taylor, A.B., Tomashevski, A., Guo, M., Hart, P.J., Diaz-Griffero, F., and Ivanov, D.N. (2012). Structure of the rhesus monkey TRIM5alpha PRYSPRY domain, the HIV capsid recognition module. Proc Natl Acad Sci USA *109*, 13278-13283.

Black, L.R., and Aiken, C. (2010). TRIM5alpha disrupts the structure of assembled HIV-1 capsid complexes in vitro. J Virol *84*, 6564-6569.

1052 Blair, W.S., Pickford, C., Irving, S.L., Brown, D.G., Anderson, M., Bazin, R., Cao, J.,
1053 Ciaramella, G., Isaacson, J., Jackson, L.*, et al.* (2010). HIV capsid is a tractable target
1054 for small molecule therapeutic intervention. PLoS Pathog *6*, e1001220.

1055 Braaten, D., Franke, E.K., and Luban, J. (1996). Cyclophilin A is required for an early
1056 step in the life cycle of human immunodeficiency virus type 1 before the initiation of
1057 reverse transcription. J Virol *70*, 3551-3560.

1058 Brennan, G., Kozyrev, Y., and Hu, S.L. (2008). TRIMCyp expression in Old World
1059 primates Macaca nemestrina and Macaca fascicularis. Proc Natl Acad Sci USA *105*,
1060 3569-3574.

1061 Briggs, J.A., Grunewald, K., Glass, B., Forster, F., Krausslich, H.G., and Fuller, S.D.
1062 (2006). The mechanism of HIV-1 core assembly: insights from three-dimensional
1063 reconstructions of authentic virions. Structure *14*, 15-20.

1064 Briggs, J.A., Simon, M.N., Gross, I., Krausslich, H.G., Fuller, S.D., Vogt, V.M., and
1065 Johnson, M.C. (2004). The stoichiometry of Gag protein in HIV-1. Nat Struct Mol Biol
1066 *11*, 672-675.

1067 Briggs, J.A., Wilk, T., Welker, R., Krausslich, H.G., and Fuller, S.D. (2003). Structural
1068 organization of authentic, mature HIV-1 virions and cores. Embo J *22*, 1707-1715.

1069 Butan, C., Winkler, D.C., Heymann, J.B., Craven, R.C., and Steven, A.C. (2008). RSV
1070 capsid polymorphism correlates with polymerization efficiency and envelope
1071 glycoprotein content: implications that nucleation controls morphogenesis. J Mol Biol
1072 *376*, 1168-1181.

1073 Byeon, I.J., Meng, X., Jung, J., Zhao, G., Yang, R., Ahn, J., Shi, J., Concel, J., Aiken,
1074 C., Zhang, P.*, et al.* (2009). Structural convergence between Cryo-EM and NMR reveals
1075 intersubunit interactions critical for HIV-1 capsid function. Cell *139*, 780-790.

1076 Caines, M.E., Bichel, K., Price, A.J., McEwan, W.A., Towers, G.J., Willett, B.J., Freund,
1077 S.M., and James, L.C. (2012). Diverse HIV viruses are targeted by a conformationally
1078 dynamic antiviral. Nature structural & molecular biology *19*, 411-416.

1079 Campbell, E.M., Perez, O., Anderson, J.L., and Hope, T.J. (2008). Visualization of a
1080 proteasome-independent intermediate during restriction of HIV-1 by rhesus
1081 TRIM5alpha. J Cell Biol *180*, 549-561.

1082 Campbell, E.M., Weingart, J., Sette, P., Opp, S., Sastri, J., O'Connor, S.K., Talley, S.,
1083 Diaz-Griffero, F., Hirsch, V., and Bouamr, F. (2015). TRIM5alpha-Mediated Ubiquitin
1084 Chain Conjugation Is Required for Inhibition of HIV-1 Reverse Transcription and Capsid
1085 Destabilization. J Virol *90*, 1849-1857.

1086 Campbell, S., and Vogt, V.M. (1995). Self-assembly in vitro of purified CA-NC proteins
1087 from Rous sarcoma virus and human immunodeficiency virus type 1. J Virol *69*, 6487-
1088 6497.

1089 Campos-Olivas, R., Newman, J.L., and Summers, M.F. (2000). Solution structure and
1090 dynamics of the Rous sarcoma virus capsid protein and comparison with capsid
1091 proteins of other retroviruses. J Mol Biol *296*, 633-649.

1092 Cornilescu, C.C., Bouamr, F., Yao, X., Carter, C., and Tjandra, N. (2001). Structural
1093 analysis of the N-terminal domain of the human T-cell leukemia virus capsid protein. J
1094 Mol Biol *306*, 783-797.

1095 Danielson, C.M., Cianci, G.C., and Hope, T.J. (2012). Recruitment and dynamics of
1096 proteasome association with rhTRIM5alpha cytoplasmic complexes during HIV-1
1097 infection. Traffic *13*, 1206-1217.

1098 Di Nunzio, F., Fricke, T., Miccio, A., Valle-Casuso, J.C., Perez, P., Souque, P., Rizzi, E.,
1099 Severgnini, M., Mavilio, F., Charneau, P.*, et al.* (2013). Nup153 and Nup98 bind the
1100 HIV-1 core and contribute to the early steps of HIV-1 replication. Virology *440*, 8-18.

1101 Diaz-Griffero, F., Kar, A., Lee, M., Stremlau, M., Poeschla, E., and Sodroski, J. (2007).
1102 Comparative requirements for the restriction of retrovirus infection by TRIM5alpha and
1103 TRIMCyp. Virology *369*, 400-410.

1104 Diaz-Griffero, F., Li, X., Javanbakht, H., Song, B., Welikala, S., Stremlau, M., and
1105 Sodroski, J. (2006a). Rapid turnover and polyubiquitylation of the retroviral restriction
1106 factor TRIM5. Virology *349*, 300-315.

1107 Diaz-Griffero, F., Qin, X.R., Hayashi, F., Kigawa, T., Finzi, A., Sarnak, Z., Lienlaf, M.,
1108 Yokoyama, S., and Sodroski, J. (2009). A B-box 2 surface patch important for
1109 TRIM5alpha self-association, capsid binding avidity, and retrovirus restriction. J Virol *83*,
1110 10737-10751.

1111 Diaz-Griffero, F., Vandegraaff, N., Li, Y., McGee-Estrada, K., Stremlau, M., Welikala, S.,
1112 Si, Z., Engelman, A., and Sodroski, J. (2006b). Requirements for capsid-binding and an
1113 effector function in TRIMCyp-mediated restriction of HIV-1. Virology *351*, 404-419.

1114 Fitzgerald, M.E., Rawling, D.C., Vela, A., and Pyle, A.M. (2014). An evolving arsenal:
1115 viral RNA detection by RIG-I-like receptors. Curr Opin Microbiol *20*, 76-81.

1116 Fletcher, A.J., Christensen, D.E., Nelson, C., Tan, C.P., Schaller, T., Lehner, P.J.,
1117 Sundquist, W.I., and Towers, G.J. (2015). TRIM5alpha requires Ube2W to anchor
1118 Lys63-linked ubiquitin chains and restrict reverse transcription. EMBO J *34*, 2078-2095.

1119 Forshey, B.M., von Schwedler, U., Sundquist, W.I., and Aiken, C. (2002). Formation of a
1120 human immunodeficiency virus type 1 core of optimal stability is crucial for viral
1121 replication. J Virol *76*, 5667-5677.

1122 Franke, E.K., and Luban, J. (1996). Inhibition of HIV-1 replication by cyclosporine A or
1123 related compounds correlates with the ability to disrupt the Gag-cyclophilin A
1124 interaction. Virology *222*, 279-282.

Franke, E.K., Yuan, H.E., and Luban, J. (1994). Specific incorporation of cyclophilin A into HIV-1 virions. Nature *372*, 359-362.

Fricke, T., Brandariz-Nunez, A., Wang, X., Smith, A.B., 3rd, and Diaz-Griffero, F. (2013). Human cytosolic extracts stabilize the HIV-1 core. J Virol *87*, 10587-10597.

Fricke, T., Buffone, C., Opp, S., Valle-Casuso, J., and Diaz-Griffero, F. (2014). BI-2 destabilizes HIV-1 cores during infection and Prevents Binding of CPSF6 to the HIV-1 Capsid. Retrovirology *11*, 120.

Gamble, T.R., Vajdos, F.F., Yoo, S., Worthylake, D.K., Houseweart, M., Sundquist, W.I., and Hill, C.P. (1996). Crystal structure of human cyclophilin A bound to the amino-terminal domain of HIV-1 capsid. Cell *87*, 1285-1294.

Ganser-Pornillos, B.K., Chandrasekaran, V., Pornillos, O., Sodroski, J.G., Sundquist, W.I., and Yeager, M. (2011). Hexagonal assembly of a restricting TRIM5alpha protein. Proc Natl Acad Sci USA *108*, 534-539.

Ganser-Pornillos, B.K., von Schwedler, U.K., Stray, K.M., Aiken, C., and Sundquist, W.I. (2004). Assembly properties of the human immunodeficiency virus type 1 CA protein. J Virol *78*, 2545-2552.

Ganser-Pornillos, B.K., Yeager, M., and Pornillos, O. (2012). Assembly and architecture of HIV. Adv Exp Med Biol *726*, 441-465.

Ganser, B.K., Li, S., Klishko, V.Y., Finch, J.T., and Sundquist, W.I. (1999). Assembly and analysis of conical models for the HIV-1 core. Science *283*, 80-83.

Goldstone, D.C., Walker, P.A., Calder, L.J., Coombs, P.J., Kirkpatrick, J., Ball, N.J., Hilditch, L., Yap, M.W., Rosenthal, P.B., Stoye, J.P.*, et al.* (2014). Structural studies of postentry restriction factors reveal antiparallel dimers that enable avid binding to the HIV-1 capsid lattice. Proc Natl Acad Sci USA *111*, 9609-9614.

Gres, A.T., Kirby, K.A., KewalRamani, V.N., Tanner, J.J., Pornillos, O., and Sarafianos, S.G. (2015). STRUCTURAL VIROLOGY. X-ray crystal structures of native HIV-1 capsid protein reveal conformational variability. Science *349*, 99-103.

Harris, R.S., Hultquist, J.F., and Evans, D.T. (2012). The restriction factors of human immunodeficiency virus. J Biol Chem *287*, 40875-40883.

Hatziioannou, T., Cowan, S., Goff, S.P., Bieniasz, P.D., and Towers, G.J. (2003). Restriction of multiple divergent retroviruses by Lv1 and Ref1. Embo J *22*, 385-394.

Hatziioannou, T., Cowan, S., Von Schwedler, U.K., Sundquist, W.I., and Bieniasz, P.D. (2004). Species-specific tropism determinants in the human immunodeficiency virus type 1 capsid. J Virol *78*, 6005-6012.

1159 Heuser, J. (1980). Three-dimensional visualization of coated vesicle formation in
1160 fibroblasts. J Cell Biol *84*, 560-583.

1161 Heymann, J.B., Butan, C., Winkler, D.C., Craven, R.C., and Steven, A.C. (2008).
1162 Irregular and semi-regular polyhedral models for Rous sarcoma virus cores. Comput
1163 Math Methods Med *9*, 197-210.

1164 Javanbakht, H., Diaz-Griffero, F., Stremlau, M., Si, Z., and Sodroski, J. (2005). The
1165 contribution of RING and B-box 2 domains to retroviral restriction mediated by monkey
1166 TRIM5alpha. J Biol Chem *280*, 26933-26940.

1167 Jin, Z., Jin, L., Peterson, D.L., and Lawson, C.L. (1999). Model for lentivirus capsid core
1168 assembly based on crystal dimers of EIAV p26. J Mol Biol *286*, 83-93.

1169 Kar, A.K., Diaz-Griffero, F., Li, Y., Li, X., and Sodroski, J. (2008). Biochemical and
1170 biophysical characterization of a chimeric TRIM21-TRIM5alpha protein. J Virol *82*,
1171 11669-11681.

1172 Khorasanizadeh, S., Campos-Olivas, R., and Summers, M.F. (1999). Solution structure
1173 of the capsid protein from the human T-cell leukemia virus type-I. J Mol Biol *291*, 491-
1174 505.

1175 Kingston, R.L., Fitzon-Ostendorp, T., Eisenmesser, E.Z., Schatz, G.W., Vogt, V.M.,
1176 Post, C.B., and Rossmann, M.G. (2000). Structure and self-association of the Rous
1177 sarcoma virus capsid protein. Structure *8*, 617-628.

1178 Kotov, A., Zhou, J., Flicker, P., and Aiken, C. (1999). Association of Nef with the human
1179 immunodeficiency virus type 1 core. J Virol *73*, 8824-8830.

1180 Kovalskyy, D.B., and Ivanov, D.N. (2014). Recognition of the HIV capsid by the
1181 TRIM5alpha restriction factor is mediated by a subset of pre-existing conformations of
1182 the TRIM5alpha SPRY domain. Biochemistry *53*, 1466-1476.

1183 Kremer, J.R., Mastronarde, D.N., and McIntosh, J.R. (1996a). Computer Visualization of
1184 Three-Dimensional Image Data Using Imod. J Struct Biol *116*, 71-76.

1185 Kremer, J.R., Mastronarde, D.N., and McIntosh, J.R. (1996b). Computer visualization of
1186 three-dimensional image data using IMOD. J Struct Biol *116*, 71-76.

1187 Kutluay, S.B., Perez-Caballero, D., and Bieniasz, P.D. (2013). Fates of retroviral core
1188 components during unrestricted and TRIM5-restricted infection. PLoS Pathog *9*,
1189 e1003214.

1190 Lamorte, L., Titolo, S., Lemke, C.T., Goudreau, N., Mercier, J.F., Wardrop, E., Shah,
1191 V.B., von Schwedler, U.K., Langelier, C., Banik, S.S.*, et al.* (2013). Discovery of novel
1192 small-molecule HIV-1 replication inhibitors that stabilize capsid complexes. Antimicrob
1193 Agents Chemother *57*, 4622-4631.

Langelier, C.R., Sandrin, V., Eckert, D.M., Christensen, D.E., Chandrasekaran, V., Alam, S.L., Aiken, C., Olsen, J.C., Kar, A.K., Sodroski, J.G.*, et al.* (2008). Biochemical characterization of a recombinant TRIM5alpha protein that restricts human immunodeficiency virus type 1 replication. J Virol *82*, 11682-11694.

Lanman, J., Lam, T.T., Emmett, M.R., Marshall, A.G., Sakalian, M., and Prevelige, P.E., Jr. (2004). Key interactions in HIV-1 maturation identified by hydrogen-deuterium exchange. Nat Struct Mol Biol *11*, 676-677.

Lee, K., Ambrose, Z., Martin, T.D., Oztop, I., Mulky, A., Julias, J.G., Vandegraaff, N., Baumann, J.G., Wang, R., Yuen, W.*, et al.* (2010). Flexible use of nuclear import pathways by HIV-1. Cell Host Microbe *7*, 221-233.

Li, S., Hill, C.P., Sundquist, W.I., and Finch, J.T. (2000). Image reconstructions of helical assemblies of the HIV-1 CA protein. Nature *407*, 409-413.

Li, X., Kim, J., Song, B., Finzi, A., Pacheco, B., and Sodroski, J. (2013). Virus-specific effects of TRIM5alpha(rh) RING domain functions on restriction of retroviruses. J Virol *87*, 7234-7245.

Li, X., and Sodroski, J. (2008). The TRIM5alpha B-box 2 domain promotes cooperative binding to the retroviral capsid by mediating higher-order self-association. J Virol *82*, 11495-11502.

Li, Y., Li, X., Stremlau, M., Lee, M., and Sodroski, J. (2006). Removal of arginine 332 allows human TRIM5alpha to bind human immunodeficiency virus capsids and to restrict infection. J Virol *80*, 6738-6744.

Li, Y., Wu, H., Wu, W., Zhuo, W., Liu, W., Zhang, Y., Cheng, M., Chen, Y.G., Gao, N., Yu, H.*, et al.* (2014). Structural insights into the TRIM family of ubiquitin E3 ligases. Cell research *24*, 762-765.

Luban, J., Bossolt, K.L., Franke, E.K., Kalpana, G.V., and Goff, S.P. (1993). Human immunodeficiency virus type 1 Gag protein binds to cyclophilins A and B. Cell *73*, 1067-1078.

Lukic, Z., Hausmann, S., Sebastian, S., Rucci, J., Sastri, J., Robia, S.L., Luban, J., and Campbell, E.M. (2011). TRIM5alpha associates with proteasomal subunits in cells while in complex with HIV-1 virions. Retrovirology *8*, 93.

Mandell, M.A., Jain, A., Arko-Mensah, J., Chauhan, S., Kimura, T., Dinkins, C., Silvestri, G., Munch, J., Kirchhoff, F., Simonsen, A.*, et al.* (2014a). TRIM proteins regulate autophagy and can target autophagic substrates by direct recognition. Dev Cell *30*, 394-409.

Mandell, M.A., Kimura, T., Jain, A., Johansen, T., and Deretic, V. (2014b). TRIM proteins regulate autophagy: TRIM5 is a selective autophagy receptor mediating HIV-1 restriction. Autophagy *10*, 2387-2388.

Matreyek, K.A., Yucel, S.S., Li, X., and Engelman, A. (2013). Nucleoporin NUP153 phenylalanine-glycine motifs engage a common binding pocket within the HIV-1 capsid protein to mediate lentiviral infectivity. PLoS Pathog *9*, e1003693.

Meehan, A.M., Saenz, D.T., Guevera, R., Morrison, J.H., Peretz, M., Fadel, H.J., Hamada, M., van Deursen, J., and Poeschla, E.M. (2014). A cyclophilin homology domain-independent role for Nup358 in HIV-1 infection. PLoS Pathog *10*, e1003969.

Meroni, G., and Diez-Roux, G. (2005). TRIM/RBCC, a novel class of 'single protein RING finger' E3 ubiquitin ligases. Bioessays *27*, 1147-1157.

Momany, C., Kovari, L.C., Prongay, A.J., Keller, W., Gitti, R.K., Lee, B.M., Gorbalenya, A.E., Tong, L., McClure, J., Ehrlich, L.S.*, et al.* (1996). Crystal structure of dimeric HIV-1 capsid protein. Nat Struct Biol *3*, 763-770.

Monroe, E.B., Kang, S., Kyere, S.K., Li, R., and Prevelige, P.E., Jr. (2010). Hydrogen/deuterium exchange analysis of HIV-1 capsid assembly and maturation. Structure *18*, 1483-1491.

Mortuza, G.B., Dodding, M.P., Goldstone, D.C., Haire, L.F., Stoye, J.P., and Taylor, I.A. (2008). Structure of B-MLV capsid amino-terminal domain reveals key features of viral tropism, gag assembly and core formation. J Mol Biol *376*, 1493-1508.

Mortuza, G.B., Haire, L.F., Stevens, A., Smerdon, S.J., Stoye, J.P., and Taylor, I.A. (2004). High-resolution structure of a retroviral capsid hexameric amino-terminal domain. Nature *431*, 481-485.

Naldini, L., Blomer, U., Gage, F.H., Trono, D., and Verma, I.M. (1996). Efficient transfer, integration, and sustained long-term expression of the transgene in adult rat brains injected with a lentiviral vector. Proc Natl Acad Sci USA *93*, 11382-11388.

Neil, S., and Bieniasz, P. (2009). Human immunodeficiency virus, restriction factors, and interferon. Journal of interferon & cytokine research : the official journal of the International Society for Interferon and Cytokine Research *29*, 569-580.

Newman, R.M., Hall, L., Kirmaier, A., Pozzi, L.A., Pery, E., Farzan, M., O'Neil, S.P., and Johnson, W. (2008). Evolution of a TRIM5-CypA splice isoform in old world monkeys. PLoS Pathog *4*, e1000003.

Nicastro, D., Schwartz, C., Pierson, J., Gaudette, R., Porter, M.E., and McIntosh, J.R. (2006). The molecular architecture of axonemes revealed by cryoelectron tomography. Science *313*, 944-948.

Nisole, S., Lynch, C., Stoye, J.P., and Yap, M.W. (2004). A Trim5-cyclophilin A fusion protein found in owl monkey kidney cells can restrict HIV-1. Proc Natl Acad Sci USA *101*, 13324-13328.

Obal, G., Trajtenberg, F., Carrion, F., Tome, L., Larrieux, N., Zhang, X., Pritsch, O., and Buschiazzo, A. (2015). STRUCTURAL VIROLOGY. Conformational plasticity of a native retroviral capsid revealed by x-ray crystallography. Science *349*, 95-98.

Ohkura, S., Yap, M.W., Sheldon, T., and Stoye, J.P. (2006). All three variable regions of the TRIM5alpha B30.2 domain can contribute to the specificity of retrovirus restriction. J Virol *80*, 8554-8565.

Perez-Caballero, D., Hatziioannou, T., Yang, A., Cowan, S., and Bieniasz, P.D. (2005). Human tripartite motif 5alpha domains responsible for retrovirus restriction activity and specificity. J Virol *79*, 8969-8978.

Pertel, T., Hausmann, S., Morger, D., Zuger, S., Guerra, J., Lascano, J., Reinhard, C., Santoni, F.A., Uchil, P.D., Chatel, L.*, et al.* (2011). TRIM5 is an innate immune sensor for the retrovirus capsid lattice. Nature *472*, 361-365.

Pettersen, E.F., Goddard, T.D., Huang, C.C., Couch, G.S., Greenblatt, D.M., Meng, E.C., and Ferrin, T.E. (2004). UCSF Chimera--a visualization system for exploratory research and analysis. Journal of computational chemistry *25*, 1605-1612.

Pornillos, O., Ganser-Pornillos, B.K., Banumathi, S., Hua, Y., and Yeager, M. (2010). Disulfide bond stabilization of the hexameric capsomer of human immunodeficiency virus. J Mol Biol *401*, 985-995.

Pornillos, O., Ganser-Pornillos, B.K., Kelly, B.N., Hua, Y., Whitby, F.G., Stout, C.D., Sundquist, W.I., Hill, C.P., and Yeager, M. (2009). X-ray structures of the hexameric building block of the HIV capsid. Cell *137*, 1282-1292.

Pornillos, O., Ganser-Pornillos, B.K., and Yeager, M. (2011). Atomic-level modelling of the HIV capsid. Nature *469*, 424-427.

Price, A.J., Jacques, D.A., McEwan, W.A., Fletcher, A.J., Essig, S., Chin, J.W., Halambage, U.D., Aiken, C., and James, L.C. (2014). Host cofactors and pharmacologic ligands share an essential interface in HIV-1 capsid that is lost upon disassembly. PLoS Pathog *10*, e1004459.

Price, A.J., Marzetta, F., Lammers, M., Ylinen, L.M., Schaller, T., Wilson, S.J., Towers, G.J., and James, L.C. (2009). Active site remodeling switches HIV specificity of antiretroviral TRIMCyp. Nat Struct Mol Biol *16*, 1036-1042.

Reymond, A., Meroni, G., Fantozzi, A., Merla, G., Cairo, S., Luzi, L., Riganelli, D., Zanaria, E., Messali, S., Cainarca, S.*, et al.* (2001). The tripartite motif family identifies cell compartments. Embo J *20*, 2140-2151.

Roa, A., Hayashi, F., Yang, Y., Lienlaf, M., Zhou, J., Shi, J., Watanabe, S., Kigawa, T., Yokoyama, S., Aiken, C.*, et al.* (2012). RING domain mutations uncouple TRIM5alpha restriction of HIV-1 from inhibition of reverse transcription and acceleration of uncoating. J Virol *86*, 1717-1727.

Rold, C.J., and Aiken, C. (2008). Proteasomal degradation of TRIM5alpha during retrovirus restriction. PLoS Pathog *4*, e1000074.

Rustagi, A., and Gale, M., Jr. (2014). Innate antiviral immune signaling, viral evasion and modulation by HIV-1. J Mol Biol *426*, 1161-1177.

Sainsbury, S., Ren, J., Saunders, N.J., Stuart, D.I., and Owens, R.J. (2008). Crystallization and preliminary X-ray analysis of CrgA, a LysR-type transcriptional regulator from pathogenic Neisseria meningitidis MC58. Acta Crystallogr Sect F Struct Biol Cryst Commun *64*, 797-801.

Salmon, P., Oberholzer, J., Occhiodoro, T., Morel, P., Lou, J., and Trono, D. (2000). Reversible immortalization of human primary cells by lentivector-mediated transfer of specific genes. Molecular therapy : the journal of the American Society of Gene Therapy *2*, 404-414.

Sanchez, J.G., Okreglicka, K., Chandrasekaran, V., Welker, J.M., Sundquist, W.I., and Pornillos, O. (2014). The tripartite motif coiled-coil is an elongated antiparallel hairpin dimer. Proc Natl Acad Sci USA *111*, 2494-2499.

Sandrin, V., Boson, B., Salmon, P., Gay, W., Negre, D., Le Grand, R., Trono, D., and Cosset, F.L. (2002). Lentiviral vectors pseudotyped with a modified RD114 envelope glycoprotein show increased stability in sera and augmented transduction of primary lymphocytes and CD34+ cells derived from human and nonhuman primates. Blood 100, 823-832.

Sayah, D.M., Sokolskaja, E., Berthoux, L., and Luban, J. (2004). Cyclophilin A retrotransposition into TRIM5 explains owl monkey resistance to HIV-1. Nature *430*, 569-573.

Schaller, T., Ocwieja, K.E., Rasaiyaah, J., Price, A.J., Brady, T.L., Roth, S.L., Hue, S., Fletcher, A.J., Lee, K., KewalRamani, V.N.*, et al.* (2011). HIV-1 capsid-cyclophilin interactions determine nuclear import pathway, integration targeting and replication efficiency. PLoS Pathog *7*, e1002439.

Sebastian, S., and Luban, J. (2005). TRIM5alpha selectively binds a restriction-sensitive retroviral capsid. Retrovirology *2*, 40.

Shi, J., Friedman, D.B., and Aiken, C. (2013). Retrovirus restriction by TRIM5 proteins requires recognition of only a small fraction of viral capsid subunits. J Virol *87*, 9271-9278.

Song, B., Gold, B., O'Huigin, C., Javanbakht, H., Li, X., Stremlau, M., Winkler, C., Dean, M., and Sodroski, J. (2005a). The B30.2(SPRY) domain of the retroviral restriction factor TRIM5alpha exhibits lineage-specific length and sequence variation in primates. J Virol *79*, 6111-6121.

Song, B., Javanbakht, H., Perron, M., Park, D.H., Stremlau, M., and Sodroski, J. (2005b). Retrovirus restriction by TRIM5alpha variants from Old World and New World primates. J Virol *79*, 3930-3937.

Sparrer, K.M., and Gack, M.U. (2015). Intracellular detection of viral nucleic acids. Curr Opin Microbiol *26*, 1-9.

Stremlau, M., Owens, C.M., Perron, M.J., Kiessling, M., Autissier, P., and Sodroski, J. (2004). The cytoplasmic body component TRIM5alpha restricts HIV-1 infection in Old World monkeys. Nature *427*, 848-853.

Stremlau, M., Perron, M., Lee, M., Li, Y., Song, B., Javanbakht, H., Diaz-Griffero, F., Anderson, D.J., Sundquist, W.I., and Sodroski, J. (2006). Specific recognition and accelerated uncoating of retroviral capsids by the TRIM5alpha restriction factor. Proc Natl Acad Sci USA *103*, 5514-5519.

Stremlau, M., Perron, M., Welikala, S., and Sodroski, J. (2005). Species-specific variation in the B30.2(SPRY) domain of TRIM5alpha determines the potency of human immunodeficiency virus restriction. J Virol *79*, 3139-3145.

Studier, F.W. (2005). Protein production by auto-induction in high density shaking cultures. Protein Expr Purif *41*, 207-234.

Thali, M., Bukovsky, A., Kondo, E., Rosenwirth, B., Walsh, C.T., Sodroski, J., and Gottlinger, H.G. (1994). Functional association of cyclophilin A with HIV-1 virions. Nature *372*, 363-365.

van Montfoort, N., Olagnier, D., and Hiscott, J. (2014). Unmasking immune sensing of retroviruses: interplay between innate sensors and host effectors. Cytokine & growth factor reviews *25*, 657-668.

Virgen, C.A., Kratovac, Z., Bieniasz, P.D., and Hatziioannou, T. (2008). Independent genesis of chimeric TRIM5-cyclophilin proteins in two primate species. Proc Natl Acad Sci USA *105*, 3563-3568.

von Schwedler, U.K., Stemmler, T.L., Klishko, V.Y., Li, S., Albertine, K.H., Davis, D.R., and Sundquist, W.I. (1998). Proteolytic refolding of the HIV-1 capsid protein amino-terminus facilitates viral core assembly. Embo J *17*, 1555-1568.

Vuillard, L., Braun-Breton, C., and Rabilloud, T. (1995). Non-detergent sulphobetaines: a new class of mild solubilization agents for protein purification. Biochem J *305 (Pt 1)*, 337-343.

Wear, M.A., Patterson, A., Malone, K., Dunsmore, C., Turner, N.J., and Walkinshaw, M.D. (2005). A surface plasmon resonance-based assay for small molecule inhibitors of human cyclophilin A. Anal Biochem *345*, 214-226.

Weinert, C., Morger, D., Djekic, A., Grutter, M.G., and Mittl, P.R. (2015). Crystal structure of TRIM20 C-terminal coiled-coil/B30.2 fragment: implications for the recognition of higher order oligomers. Sci Rep *5*, 10819.

Welker, R., Hohenberg, H., Tessmer, U., Huckhagel, C., and Krausslich, H.G. (2000). Biochemical and structural analysis of isolated mature cores of human immunodeficiency virus type 1. J Virol *74*, 1168-1177.

Wilson, S.J., Webb, B.L., Maplanka, C., Newman, R.M., Verschoor, E.J., Heeney, J.L., and Towers, G.J. (2008). Rhesus macaque TRIM5 alleles have divergent antiretroviral specificities. J Virol *82*, 7243-7247.

Wu, X., Anderson, J.L., Campbell, E.M., Joseph, A.M., and Hope, T.J. (2006). Proteasome inhibitors uncouple rhesus TRIM5alpha restriction of HIV-1 reverse transcription and infection. Proc Natl Acad Sci USA *103*, 7465-7470.

Yamauchi, K., Wada, K., Tanji, K., Tanaka, M., and Kamitani, T. (2008). Ubiquitination of E3 ubiquitin ligase TRIM5 alpha and its potential role. Febs J *275*, 1540-1555.

Yang, H., Ji, X., Zhao, G., Ning, J., Zhao, Q., Aiken, C., Gronenborn, A.M., Zhang, P., and Xiong, Y. (2012). Structural insight into HIV-1 capsid recognition by rhesus TRIM5alpha. Proc Natl Acad Sci USA *109*, 18372-18377.

Yap, M.W., Nisole, S., and Stoye, J.P. (2005). A single amino acid change in the SPRY domain of human Trim5alpha leads to HIV-1 restriction. Curr Biol *15*, 73-78.

Yee, J.K., Friedmann, T., and Burns, J.C. (1994). Generation of high-titer pseudotyped retroviral vectors with very broad host range. Methods Cell Biol 43 Pt A, 99-112.

Ylinen, L.M., Price, A.J., Rasaiyaah, J., Hue, S., Rose, N.J., Marzetta, F., James, L.C., and Towers, G.J. (2010). Conformational adaptation of Asian macaque TRIMCyp directs lineage specific antiviral activity. PLoS Pathog *6*, e1001062.

Yoo, J.S., Kato, H., and Fujita, T. (2014). Sensing viral invasion by RIG-I like receptors. Curr Opin Microbiol *20*, 131-138.

Yoo, S., Myszka, D.G., Yeh, C., McMurray, M., Hill, C.P., and Sundquist, W.I. (1997). Molecular recognition in the HIV-1 capsid/cyclophilin A complex. J Mol Biol *269*, 780-795.

Yu, Z., Dobro, M.J., Woodward, C.L., Levandovsky, A., Danielson, C.M., Sandrin, V., Shi, J., Aiken, C., Zandi, R., Hope, T.J.*, et al.* (2013). Unclosed HIV-1 capsids suggest a curled sheet model of assembly. J Mol Biol *425*, 112-123.

Yudina, Z., Roa, A., Johnson, R., Biris, N., de Souza Aranha Vieira, D.A., Tsiperson, V., Reszka, N., Taylor, A.B., Hart, P.J., Demeler, B.*, et al.* (2015). RING Dimerization Links Higher-Order Assembly of TRIM5alpha to Synthesis of K63-Linked Polyubiquitin. Cell reports *12*, 788-797.

Zhang, W., Cao, S., Martin, J.L., Mueller, J.D., and Mansky, L.M. (2015). Morphology and ultrastructure of retrovirus particles. AIMS biophysics *2*, 343-369.

Zhao, G., Ke, D., Vu, T., Ahn, J., Shah, V.B., Yang, R., Aiken, C., Charlton, L.M., Gronenborn, A.M., and Zhang, P. (2011). Rhesus TRIM5alpha disrupts the HIV-1 capsid at the inter-hexamer interfaces. PLoS Pathog *7*, e1002009.

Zhao, G., Perilla, J.R., Yufenyuy, E.L., Meng, X., Chen, B., Ning, J., Ahn, J., Gronenborn, A.M., Schulten, K., Aiken, C.*, et al.* (2013). Mature HIV-1 capsid structure by cryo-electron microscopy and all-atom molecular dynamics. Nature *497*, 643-646.

Zheng, S.Q., Keszthelyi, B., Branlund, E., Lyle, J.M., Braunfeld, M.B., Sedat, J.W., and Agard, D.A. (2007). UCSF tomography: an integrated software suite for real-time electron microscopic tomographic data collection, alignment, and reconstruction. J Struct Biol *157*, 138-147.

Zlotnick, A., Stahl, S.J., Wingfield, P.T., Conway, J.F., Cheng, N., and Steven, A.C. (1998). Shared motifs of the capsid proteins of hepadnaviruses and retroviruses suggest a common evolutionary origin. FEBS Lett *431*, 301-304.

Acknowledgements

Deep-etch electron microscopy was performed by Robyn Roth and John Heuser at the Laboratory of Electron Microscopy Sciences, Department of Cell Biology, Washington University School of Medicine. We are grateful to Ruth Pumroy for contributing TRIM5 proteins used in our co-assembly assays and to members of our laboratories for helpful discussions and critical reading of the manuscript. This work was supported by funds from NIH NIGMS P50 082545 (to MY, BKG-P GJJ and WIS).

FIGURE CAPTIONS

Figure 1. ECT analysis of TRIM5-21R 2D crystals. (A) Schematic of the TRIM5 dimer. The two RING (yellow) and B-box 2 (red) domains are separated by a ~17 nm, antiparallel dimeric coiled-coil (blue). The two L2 linkers (green) fold back towards the 2-fold axis of the coiled-coil to orient two capsid-binding SPRY domains (orange). (B) Schematic of the TRIM5 hexagonal lattice model. (C and D) Tomographic slice (top) of (C) full-length TRIM5-21R, and (D) TRIM5-21R$_{\Delta SPRY}$ lattices. Scale bars are 100 nm. In both cases, the computed Fourier transform (bottom, left) and sub-tomogram average without imposed rotational symmetry (bottom, middle) exhibits six-fold symmetry. Iso-surface representations of the densities are also shown (bottom, right). (E) A density difference map of the sub-tomogram averages of full-length TRIM5-21R and TRIM5-21R$_{\Delta SPRY}$ lattices reveals positive density (red) at the center of each hexagon edge, corresponding to the SPRY domain position, supporting the TRIM5α dimer model shown in (A). (F) Heat maps (bottom) of lattice arm lengths and angles measured from refined lattice points (top) selected from the TRIM5-21R tomogram in (C). (G) Histograms showing the distributions of measured arm lengths (n=155) and angles (n=111). The most abundant arm length (18.5-19 nm) and arm angle (120°) are consistent with the structure model in (A) and the p6 plane group symmetry of TRIM5-21R 2D crystals (Ganser-Pornillos et al., 2011), respectively. Note that this analysis probably underestimates the extent of hexamer variability owing to the initial selection of well-ordered lattice points.

Figure 2. Purification and characterization of recombinant TRIM5 proteins. (A) Coomassie-stained SDS-PAGE showing the stepwise purification of rhesus TRIM5α (TRIM5α_{rh}). Samples correspond to: soluble lysate from control SF9 cells (Uninfected, lane 1); soluble lysate from SF9 cells expressing OSF-TRIM5α_{rh} (Infected, lane 2); StrepTactin affinity-purified OSF-TRIM5α_{rh} (Affinity, lane 3); TRIM5α_{rh} after removal of the OSF tag by PreScission protease treatment (Tag Cleavage, lane 4); dimeric TRIM5α_{rh} purified by Q anion exchange chromatography (Anion Exchange, lane 5); dimeric TRIM5α_{rh} purified by Superdex 200 gel filtration chromatography (Gel Filtration, lane 6). (B) Coomassie-stained SDS-PAGE showing 1.5 µg of purified rhesus, African green monkey pygerythrus (AGMpyg), chimpanzee TRIM5α, proteolysis-resistant owl monkey TRIMCyp$_{K283D,Q287D}$, human TRIM5α, and HIV-1-restricting human TRIM5α_{R332P}. (C, D) TRIM5 hexagonal assembly is a conserved property of primate TRIM5 proteins. Negatively stained EM image of hexagonal arrays formed by (C) TRIM5α_{AGMpyg} and (D) TRIMCyp. Computed Fourier transforms (top right insets) show clear hexagonal order and filtered projection density maps of 2-dimensional crystals (bottom left insets) also reveal hexagonal rings and density distributions reminiscent of TRIM5-21R lattices (Ganser-Pornillos et al., 2011). The unit cell parameters are a = 345 Å, b = 345 Å, γ = 120° (TRIM5α_{AGMpyg}); and a = 345 Å, b = 344 Å, γ = 119° (TRIMCyp). Note that the TRIMCyp samples contained a mixture of full-length TRIMCyp and fragments that were proteolyzed to the C-terminus of residues K283 or Q287 (see Results and Materials and Methods for details). The relatively thinner 2-fold density in the TRIMCyp projection map could either reflect low crystal occupancy of the CypA

1480 domain (due to proteolysis) or inherently flexible CypA domains in TRIMCyp as has
1481 been proposed by (Goldstone et al., 2014).
1482
1483 **Figure 2 – figure supplement 1. HIV-1 CA restriction activity of different TRIM5**
1484 **alleles.** HeLa-M cells were transduced with vectors expressing TRIM5α_{hu}, TRIM5α_{cpz},
1485 TRIM5α_{AGMpyg}, TRIM5α_{rh}, TRIMCyp, or TRIMCyp$_{K283D,Q287D}$. Cells express TRIM5
1486 proteins at approximate similar levels as verified by western blotting with α-TRIM5α
1487 antibody (bottom). Integrated band intensities for this blot were calculated and
1488 normalized to the value of TRIM5α_{rh}: 0.5 (TRIM5α_{hu}), 1.0 (TRIM5α_{rh}), 1.3 (TRIMCyp,
1489 upper band), 1.3 (TRIMCyp$_{K283D,Q287D,}$ upper band), 1.8 (TRIM5α_{cpz}) and 3.2
1490 (TRIM5α_{AGMpyg}). Cells were transduced with VSV-G pseudotyped HIV-GFP reporter
1491 virions at the designated MOI levels (top). Percentages of infected cells (GFP positive
1492 cells) were determined by FACS. As expected, TRIM5 proteins from AGMpyg, rhesus
1493 and owl monkey restricted HIV-1 whereas human and chimpanzee TRIM5 did not. Note
1494 also that introduction of proteolysis-resistant mutations (K283D, Q287D) into TRIMCyp
1495 did not affect restriction. Each experiment was repeated twice with similar results.
1496
1497 **Figure 3. Assembly of restricting TRIM5 proteins on 2D crystals of HIV-1 CA.**
1498 Negative stain EM images of CA 2D crystals decorated with (A) TRIM5α_{rh}, (B)
1499 TRIMCyp$_{K283D,Q287D}$, (C) TRIM5α_{hu} (non-restricting isoform), (D) TRIM5$\alpha_{hu,R332P}$
1500 (restricting mutant). Scale bars are 100 nm. Computed Fourier transforms (insets) and
1501 indexing (second insets) show the first and second order reflections of two CA lattices

and their unit cell parameters (red and blue) as well as diffraction spots (A, B) or rings (C) corresponding to the first order reflections of the TRIM5 lattices (green).

Figure 4. Assembly of TRIM5α proteins on HIV-1 CA tubes. (A) Deep-etch electron micrographs of control hyperstable CA tubes (top) and TRIM5α decorated CA tubes (bottom) with blow-up views of boxed regions to the right. Scale bar is 50 nm. (B) Negative stain electron micrographs of co-assembled TRIM5α_{AGMpyg}-coated CA tubes (top). Scale bar is 100 nm. Expanded views of negatively stained CA assembly in the absence (bottom left) or presence of TRIM5α_{AGMpyg} proteins (bottom right). TRIM5α formed ring-like decorations (yellow arrows) on the tube surface and displayed protrusions along the edge of the tube (red arrows). Similar decorations were not observed in the control case. The protrusions were regularly spaced and we speculate that they are either well-ordered coiled-coil arms from adjacent hexagons wrapping around the CA tubes or possibly ordered RING domains projecting outward from the lattice. Scale bars are 50 nm. (C) Histograms showing the distributions of measured inter-ring spacings in the TRIM5α_{AGMpyg}–decorated tubes (blue bars, n=170) and in co-assemblies (red bars, n=164), and of inter-protrusion spacings in co-assemblies (green bars, n=166). The most abundant inter-ring spacing (30-35 nm) is consistent with the spacing of TRIM5-21R 2D crystals, indicating similar structures. (D) Electron cryotomography (ECT) reveals that TRIM5α forms hexagonal nets on the surface of CA tube. Hexagon-like rings are marked by magenta arrows. Scale bar is 80 nm. (E) Histograms showing the distributions of arm lengths (n=35) and angles (n=42) measured from three-fold vertex in ECT.

Figure 4 – figure supplement 1. TRIM5 protein binding to hyperstable HIV-1 CA tubes. (A) (left) Sucrose co-sedimentation binding experiments were performed using either wild type, full-length TRIM5α$_{AGMpyg}$ (Wild Type, lanes 1, 2), or a truncated TRIM5α$_{AGMpyg}$ that lacked the SPRY domain (ΔSPRY, lanes 3, 4), in the absence (lanes 1, 3) or presence of CA tubes (lanes 2, 4). Pelletable CA and associated TRIM5α$_{AGMpyg}$ (Pellet, 30% in total), were separated from unassembled and soluble CA proteins and unbound TRIM5α$_{AGMpyg}$ (Supernatant, 3% of total) by centrifugation through a sucrose cushion, and analyzed by western blotting, with the input levels of both proteins shown for reference (Input, 3% of total). (right) Analogous experiments performed with proteolysis-resistant TRIMCyp$_{K283D,Q287D}$ in the absence (lane 5) or presence (lanes 6, 7) of helical CA tubes, without (lanes 5, 6) or with added cyclosporine A (CsA) (lane 7), a competitive inhibitor of the CypA-CA interaction. Lane 8 is a CA tube control, with no added TRIMCyp$_{K283D,Q287D}$ or CsA. Representative results from one of three independent experiments are shown. (B) Representative electron micrographs of control HIV-1 CA tubes, and tubes decorated with different TRIM5α or TRIMCyp$_{K283D,Q287D}$ and negatively stained with Uranyl Acetate (UA) or Phosphotungstate (PTA). Scale bars are 50 nm.

Figure 5. Purification of wild type and hyperstable HIV-1 cores. (A) Sucrose-gradient purification profiles of wild type (left) and hyperstable A14C/E45C (right) HIV-1 cores (Kotov et al., 1999). (top) α-CA western blots of sucrose gradient fractions, (bottom) graph showing quantified CA levels and solution density (bottom blue line;

g/ml) in each gradient fraction. The higher stability of crosslinked HIV-1 cores can be seen by comparing the amounts of wild type and $CA_{A14C/E45C}$ in fractions 10-12 (pink regions). Core-containing fractions were pooled, washed, and concentrated for the analyses in B and C. The experiment was repeated at least three times with similar results. (B) Negative stain electron micrograph of wild type (left) and $CA_{A14C/E45C}$ (right) cores. Pie charts (inset) of observed morphologies of wild type (left; n = 143 cores) and $CA_{A14C/E45C}$ cores (right; n=353 cores) reveal that the introduced Cys crosslinks do not alter HIV-1 core morphologies significantly. (C) Non-reducing α-CA western blots showing that $CA_{A14C/E45C}$ cores are crosslinked (compare % hexamer as a function of [β-ME]). Asterisks indicate unprocessed Gag fragments (p55 and p41) that co-purifed with mature cores during purification. (D, E) Negative stain electron micrographs showing the relative abundance and purity of cores purified by the affinity method. (D) $CA_{A14C/E45C}$ crosslinked cores and (E) $CA_{A14C/E45C/A92E}$ crosslinked cores. Note that the additional A92E mutation reduced core clustering. Scale bar is 100 nm.

Figure 5 – figure supplement 1. Hyperstable core particle characterization and purification. (A-C) $CA_{A14C/E45C}$ assemblies in fractions 7-9 are also composed of crosslinked hexamers. (A) Non-reducing α-CA western blot of $CA_{A14C/E45C}$ assemblies in fractions 7-9. (B) Negative stain electron micrograph of fractions 7-9. (C) Pie chart showing the atypical morphological distribution of particles in fractions 7-9. (D-E) HIV-1 core affinity purification and characterization. (D) Purification scheme (key at right). Pure, recombinant OneSTrEP-FLAG-cyclophilin A (OSF-CypA) was added to HIV-1 virions and their limiting membrane was stripped by detergent treatment. OSF-CypA-

core complexes were captured using Strep-Tactin sepharose magnetic beads. The beads were restrained magnetically and vesicles and other bound contaminants were removed by rigorous washing. Cores (but not CypA) were then eluted by addition of cyclosporine A. (E) α-CA (top) and α-FLAG (CypA; bottom) western blots of samples from different steps in HIV-1 core affinity purification (see Experimental Procedures for details). Note that the eluate, which contains purified cores, is free from bound CypA. (F) SDS-PAGE gel with silver staining reveals that the expected protein components of HIV-1 cores are all present in purified hyperstable cores.

Figure 6. TRIM5α proteins bind directly to HIV-1 cores. (A) Sucrose cushion co-sedimentation binding assay for TRIM5α-HIV-1 core interactions. TRIM5α proteins were incubated in the absence of cores (lanes 1, 3, 5) or in the presence of hyperstable HIV-1 cores (lanes 2, 4, 6). Sucrose cushion centrifugation binding experiments were performed, and pelletable cores and bound TRIM5α (Pellet, 30% of total) and unbound TRIM5α (Supernatant, 2% of total) were analyzed by western blotting for TRIM5α and CA proteins. The input levels of both proteins are also shown for reference (Input, 2% of total). Representative results from one of three independent experiments are shown. (B) Representative electron micrographs of control HIV-1 cores (first row), and cores decorated with TRIM5α_{rh} (second row) and negatively stained with Uranyl Acetate. TRIM5α decorations were highlighted in yellow (third row). Scale bars are 50 nm.

Figure 7. ECT reveals that TRIM5α forms flexible hexagonal nets on hyperstable HIV-1 cores. (A) Segmented HIV-1 core (yellow) decorated with TRIM5α (blue). (B)

Segmented HIV-1 core decorated with TRIM5α and subjected to mild sulfo-EGS crosslinking prior to vitrification. (C) TRIM5α structural model docked into the cryoEM volume of the tomogram shown in (B). (D) Idealized schematic model of an HIV-1 fullerene cone bound by a TRIM5α hexagonal net. Scale bars are 35 nm.

Figure 7 – figure supplement 1. ECT of hyperstable HIV-1 cores. (A) Tomographic slices of four representative HIV-1 cores, displaying no densities above background noise around their exterior. A hole at the tip is marked by an orange asterisk (Yu et al., 2013). Scale bar is 50 nm. (B, C) Tomographic slices of non-linear anisotropic diffusion (NAD)-filtered cores display side- and front-facing views of individual CA hexamers. Blow-up views show densities with dimensions similar to those of the crystal structure of the HIV-1 CA hexamer. (D) Crystal structure of the HIV-1 CA hexamer whose dimensions match those of the densities highlighted in (B) and (C).

Figure 7 – figure supplement 2. ECT of a HIV-1 hyperstable core in complex with TRIM5α. (A-H) Series of slices through the Z axis of a tomogram of one HIV-1 core, displaying densities above background noise around their exterior (sulfo-EGS crosslinked). The tomograms were SIRT reconstructed and NAD filtered. Slice numbers are indicated in the bottom left corner of each frame. Scale bars are 50 nm. (I) Segmentation of the tomogram shown in (A-H) reveals the distribution of TRIM5α (blue) on the HIV-1 core surface (yellow).

Figure 7 – figure supplement 3. Characterization of TRIM5 hexagonal nets on HIV-1 cores. Histograms showing the distribution of arm lengths (n=51, top) and angles (n=68, bottom) of TRIM5 hexamers in ECT.

VIDEO DESCRIPTION

Video 1. HIV-1 CA tube co-assembled with TRIM5α and crosslinked.

ECT of HIV-1 CA tube (yellow) decorated with TRIM5α (blue). Video corresponds to Figure 4D.

Video 2. HIV-1 core decorated with TRIM5α (without crosslinking).

ECT of HIV-1 core (yellow) decorated with TRIM5α (blue). Video corresponds to Figure 7A.

Video 3. TRIM5α-HIV-1 cores associated with the air/water interface.

Representative ECT showing the interaction of TRIM5α-HIV-1 cores with the air/water interface. Video corresponds to Figure 7.

Video 4. HIV-1 core decorated with TRIM5α and crosslinked. HIV-1 core (yellow) decorated with TRIM5α (blue) were subjected to crosslinking and imaged by ECT. Video corresponds to Figure 7B and 7C.

SUPPLEMENTARY FILE DESCRIPTION

Supplementary file 1. (A) List of plasmids used in this study. (B) TRIM5 constructs and their molecular weights.

Figure 1

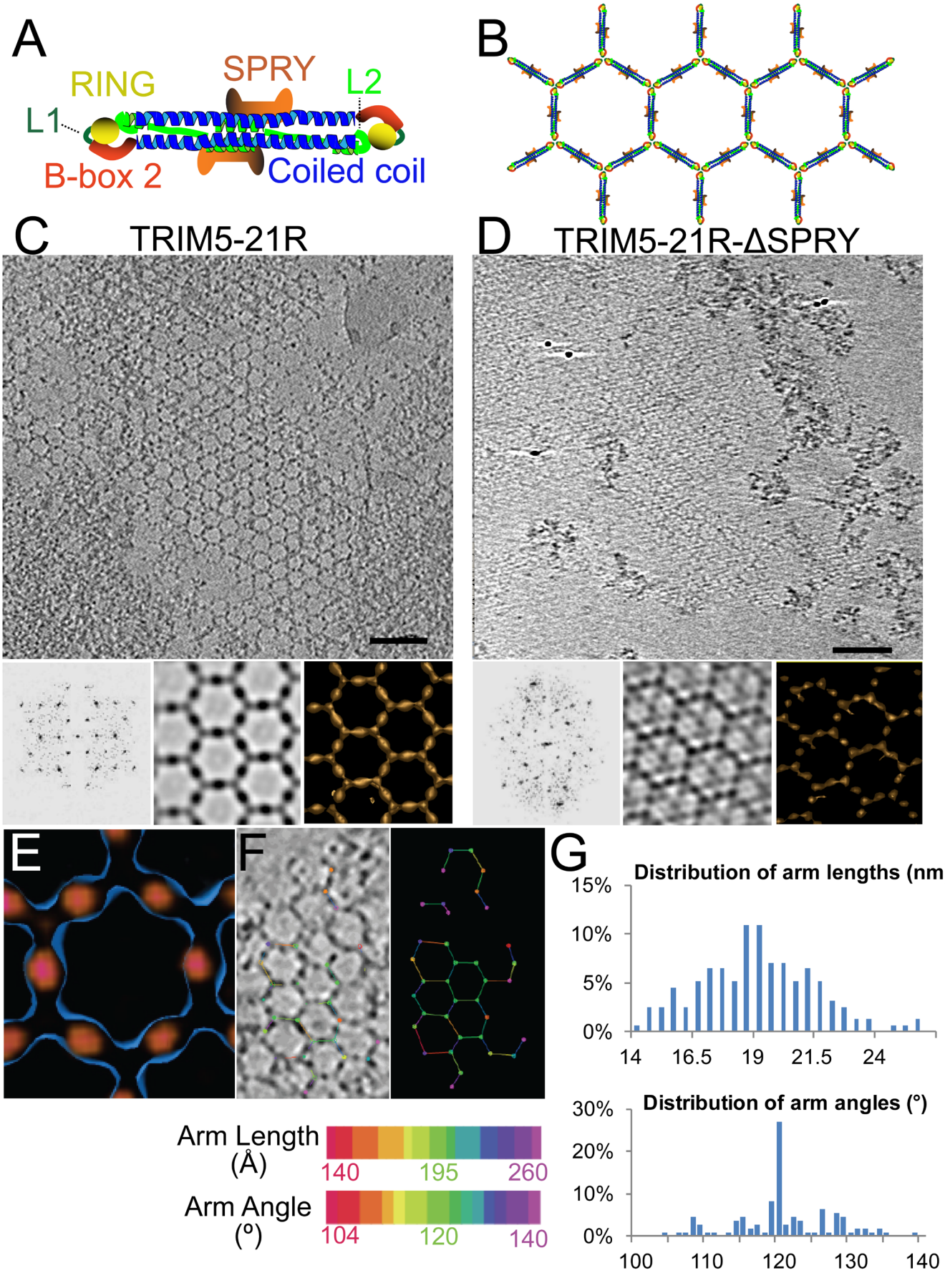
A
RING
SPRY
L2
L1
B-box 2
Coiled coil
B
C
TRIM5-21R
D
TRIM5-21R-ΔSPRY
E
F
G
Distribution of arm lengths (nm)
15%
10%
5%
0%
14
16.5
19
21.5
24
Distribution of arm angles (°)
30%
20%
10%
0%
100
110
120
130
140
Arm Length (Å)
140
195
260
Arm Angle (°)
104
120
140

Figure 2

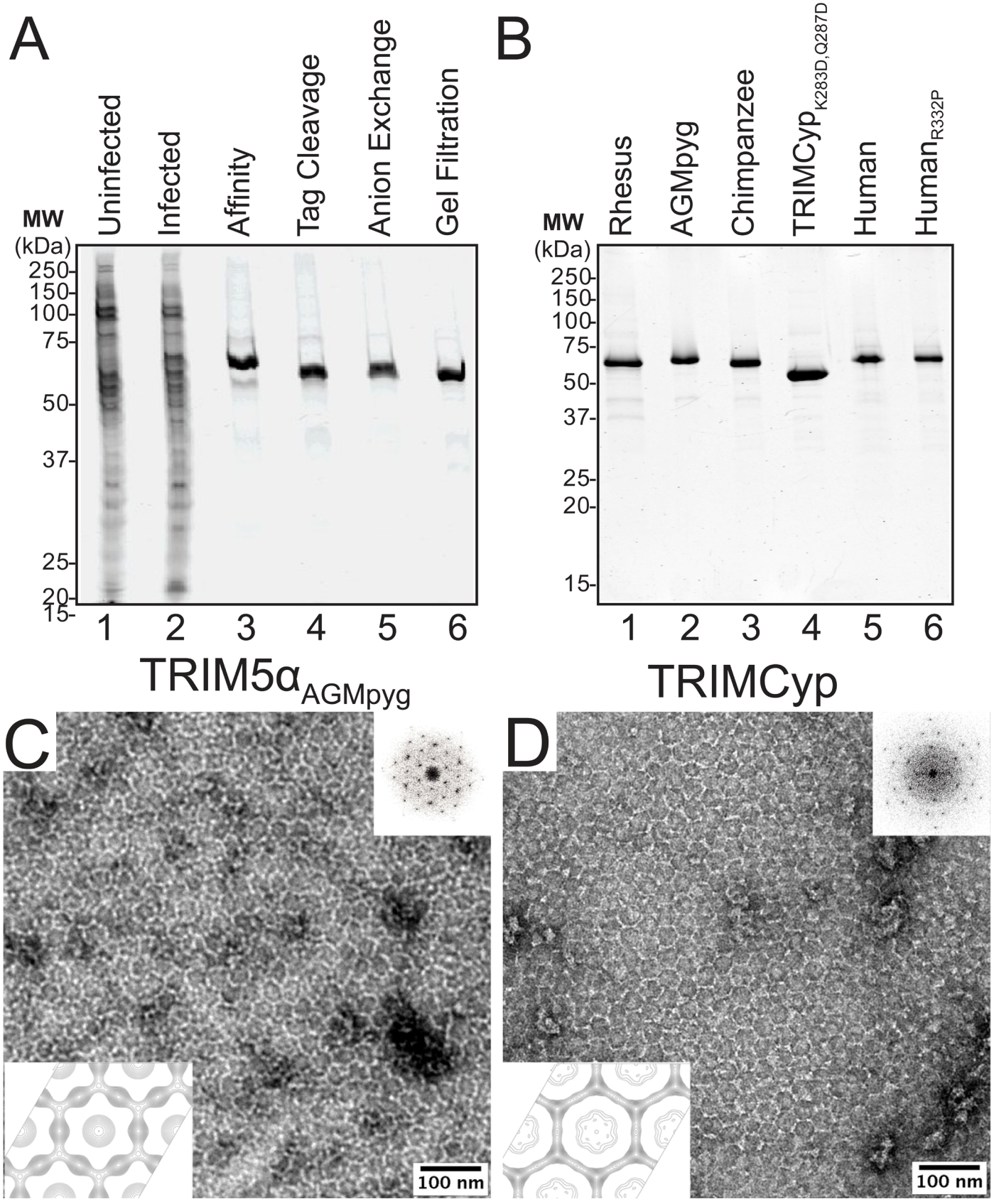
A
Uninfected
Infected
Affinity
Tag Cleavage
Anion Exchange
Gel Filtration
MW
(kDa)
250
150
100
75
50
37
25
20
15
1
2
3
4
5
6
TRIM5α AGMpyg
B
Rhesus
AGMpyg
Chimpanzee
TRIMCyp K283D, Q287D
Human
Human R332P
MW
(kDa)
250
150
100
75
50
37
25
20
15
1
2
3
4
5
6
TRIMCyp
C
100 nm
D
100 nm

Figure 3

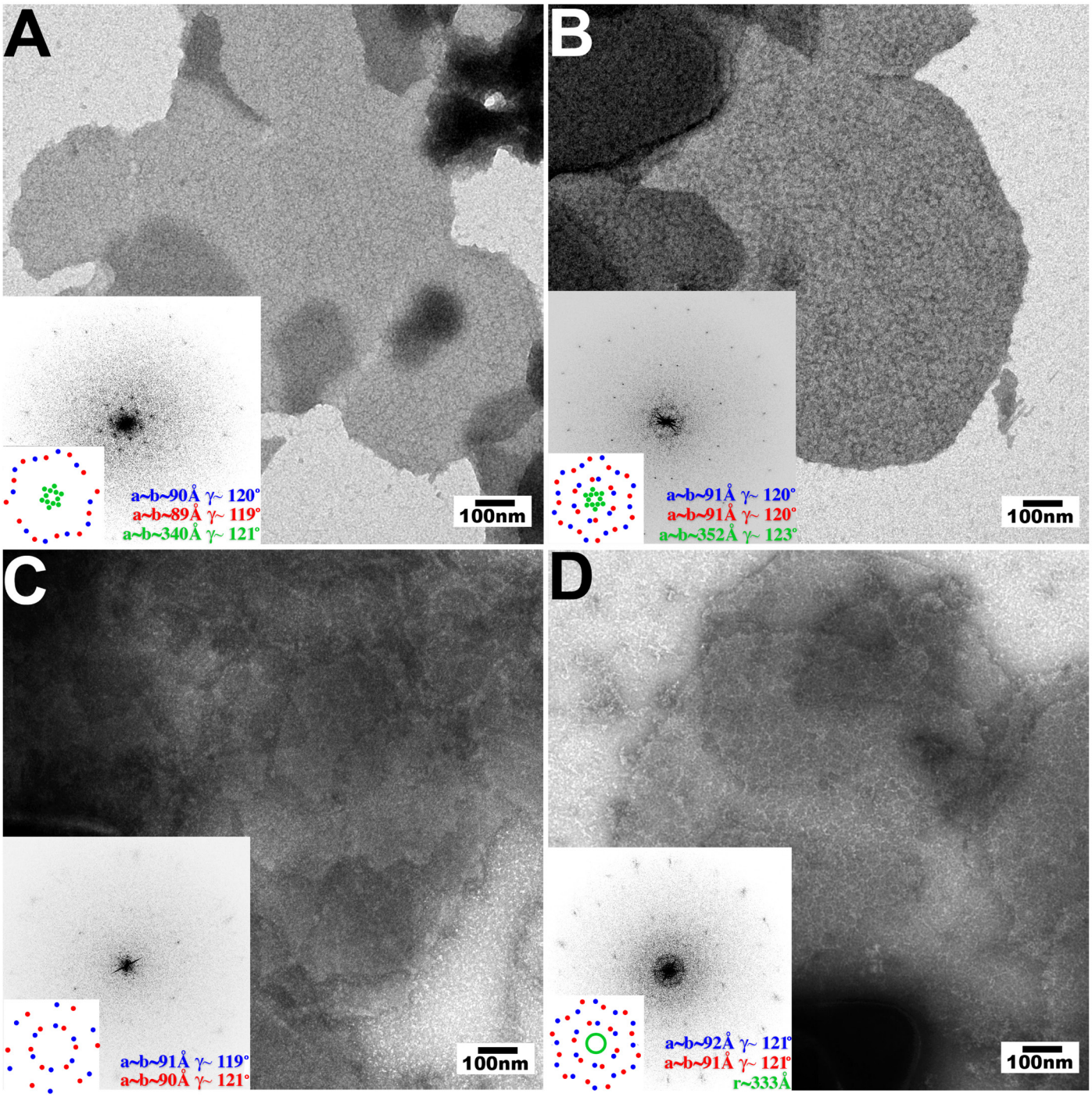
A
a~b~90Å γ~ 120°
a~b~89Å γ~ 119°
a~b~340Å γ~ 121°
100nm
B
a~b~91Å γ~ 120°
a~b~91Å γ~ 120°
a~b~352Å γ~ 123°
100nm
C
a~b~91Å γ~ 119°
a~b~90Å γ~ 121°
100nm
D
a~b~92Å γ~ 121°
a~b~91Å γ~ 121°
r~333Å
100nm

Figure 4

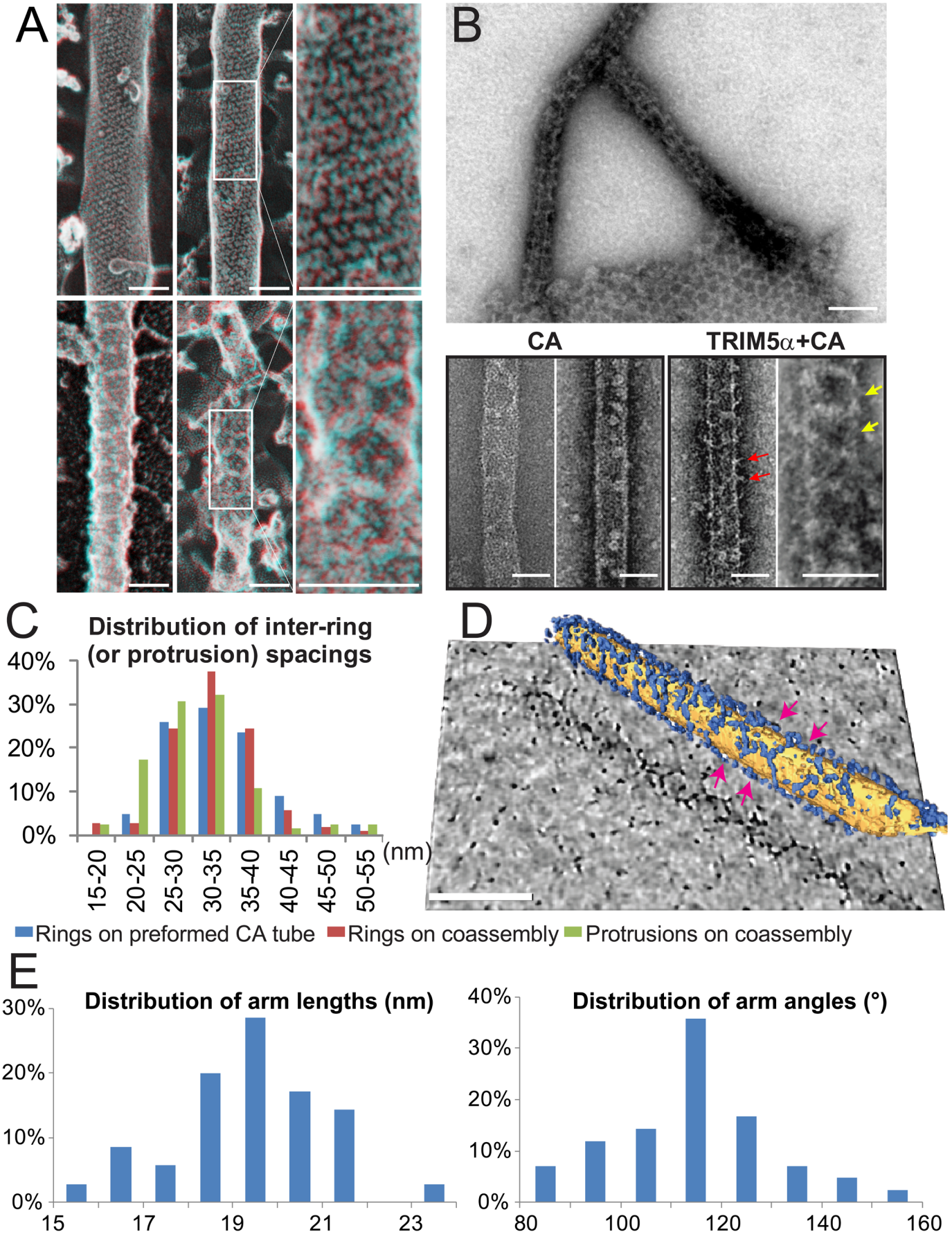
A
B
CA
TRIM5α+CA
C
Distribution of inter-ring (or protrusion) spacings
40%
30%
20%
10%
0%
15-20
20-25
25-30
30-35
35-40
40-45
45-50
50-55
(nm)
D
Rings on preformed CA tube
Rings on coassembly
Protrusions on coassembly
E
Distribution of arm lengths (nm)
30%
20%
10%
0%
15
17
19
21
23
Distribution of arm angles (°)
40%
30%
20%
10%
0%
80
100
120
140
160

Figure 5

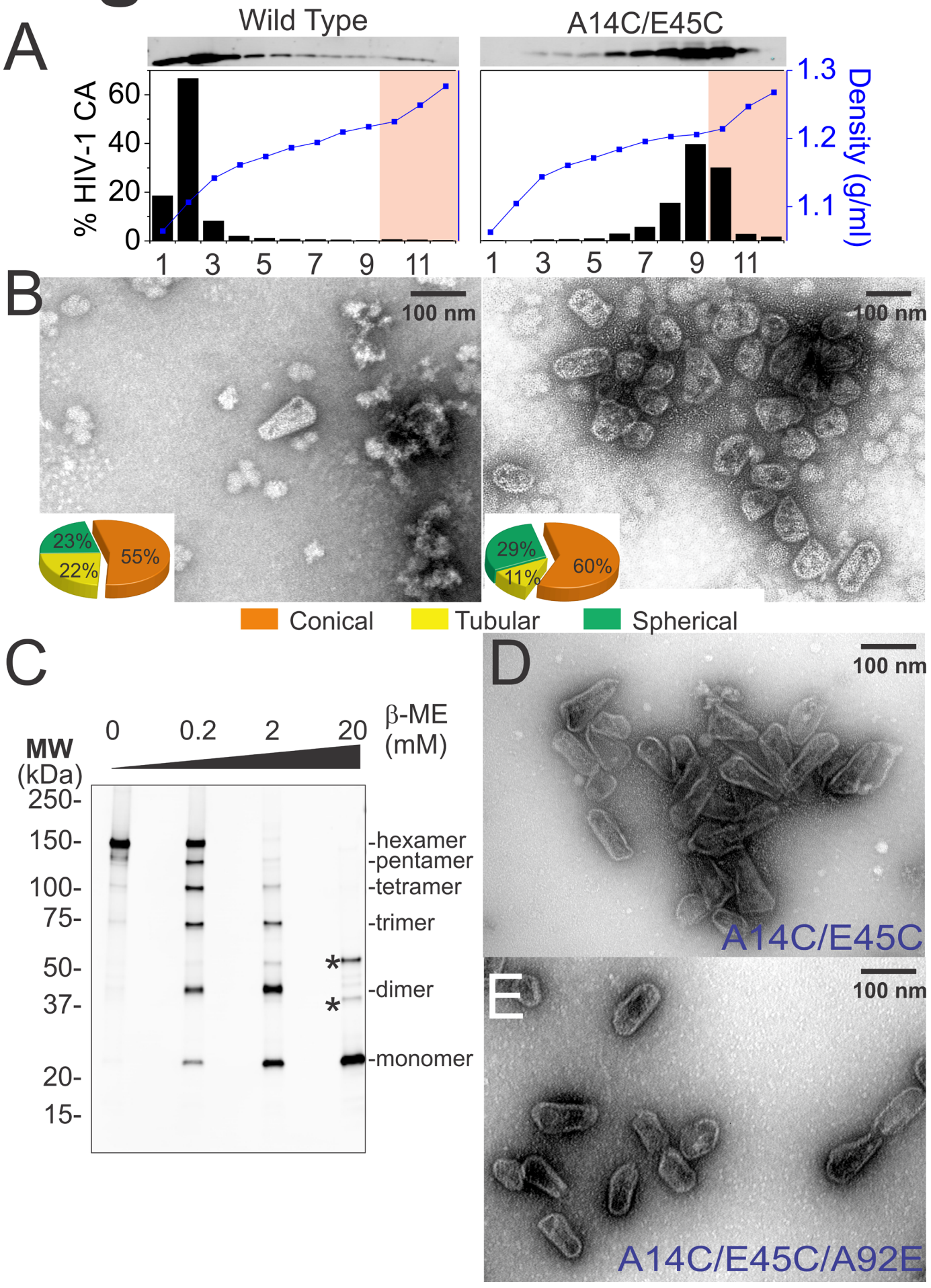
A
Wild Type
A14C/E45C
% HIV-1 CA
60
40
20
0
1 3 5 7 9 11
1.3
1.2
1.1
Density (g/ml)
B
100 nm
23%
22%
55%
29%
11%
60%
Conical
Tubular
Spherical
C
MW
(kDa)
250-
150-
100-
75-
50-
37-
20-
15-
0
0.2
2
20
β-ME
(mM)
-hexamer
-pentamer
-tetramer
-trimer
-dimer
-monomer
*
*
D
100 nm
A14C/E45C
E
100 nm
A14C/E45C/A92E

Figure 6

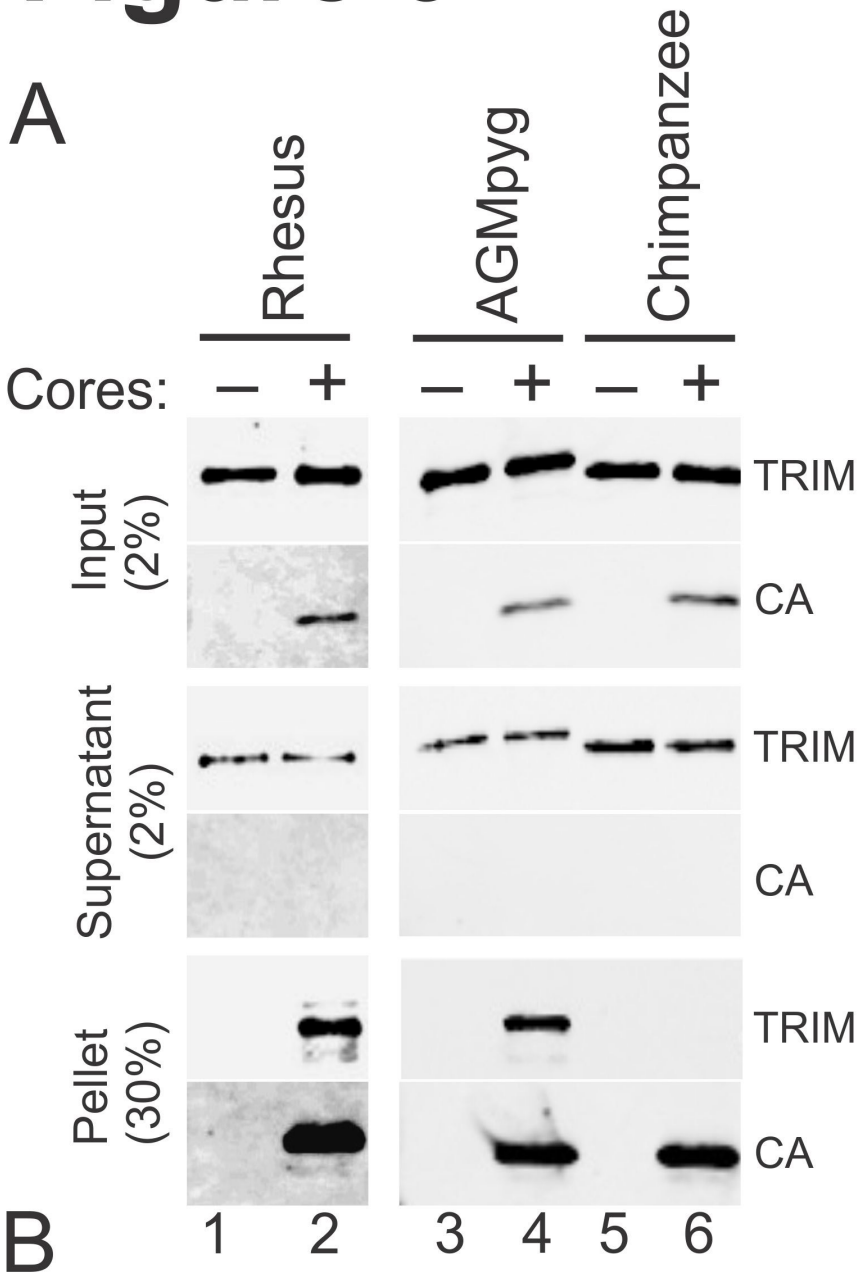
A
Rhesus
AGMpyg
Chimpanzee
Cores:
– + – + – +
Input (2%)
Supernatant (2%)
Pellet (30%)
TRIM
CA
TRIM
CA
TRIM
CA
1 2 3 4 5 6
B

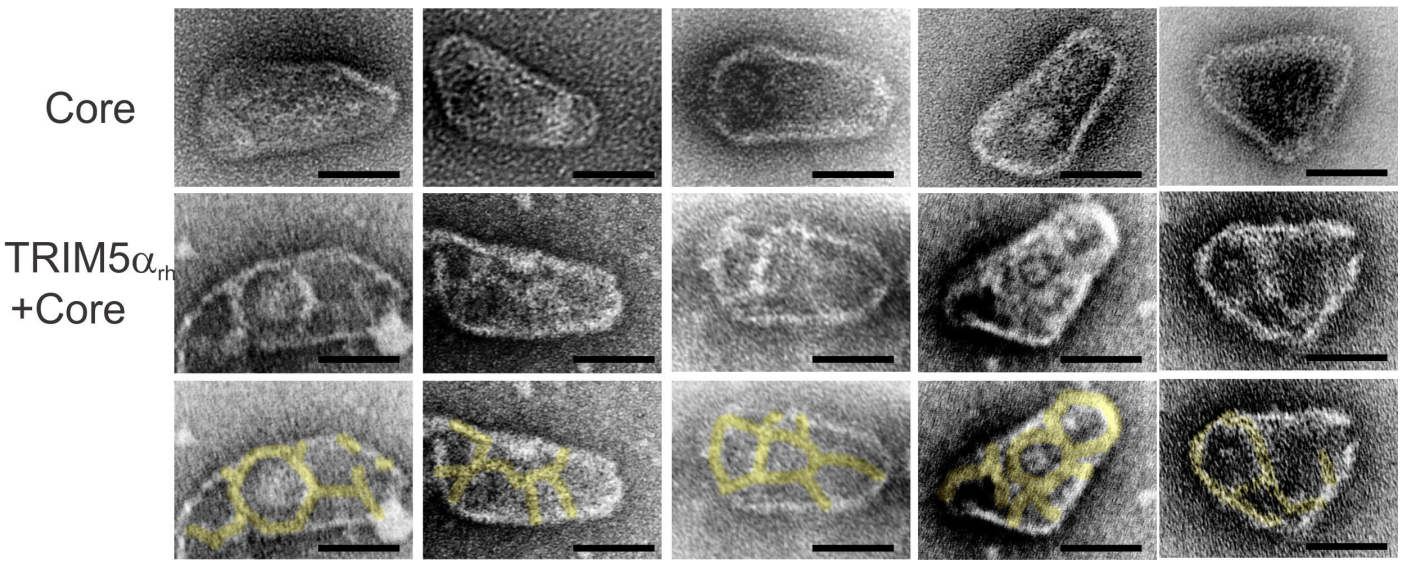
Core
TRIM5α$_{rh}$ +Core

Figure 7